10-18-2005

1/*d* Expansion for *k*-Core Percolation

A. Brooks Harris
University of Pennsylvania, harris@sas.upenn.edu

Jürgen M. Schwarz
University of Pennsylvania

$1/d$ Expansion for k-Core Percolation

Abstract
The physics of k-core percolation pertains to those systems whose constituents require a minimum number of k connections to each other in order to participate in any clustering phenomenon. Examples of such a phenomenon range from orientational ordering in solid ortho-para H_2 mixtures to the onset of rigidity in bar-joint networks to dynamical arrest in glass-forming liquids. Unlike ordinary (k=1) and biconnected (k=2) percolation, the mean field $k \geqslant 3$-core percolation transition is both continuous *and* discontinuous, i.e., there is a jump in the order parameter accompanied with a diverging length scale. To determine whether or not this hybrid transition survives in finite dimensions, we present a $1/d$ expansion for k-core percolation on the d-dimensional hypercubic lattice. We show that to order $1/d^3$ the singularity in the order parameter and in the susceptibility occur at the same value of the occupation probability. This result suggests that the unusual hybrid nature of the mean field k-core transition survives in high dimensions.

Disciplines
Physics

$1/d$ expansion for k-core percolation

A. B. Harris and J. M. Schwarz
Department of Physics and Astronomy, University of Pennsylvania, Philadelphia, Pennsylvania 19104, USA
(Received 2 June 2005; published 18 October 2005)

The physics of k-core percolation pertains to those systems whose constituents require a minimum number of k connections to each other in order to participate in any clustering phenomenon. Examples of such a phenomenon range from orientational ordering in solid ortho-para H_2 mixtures to the onset of rigidity in bar-joint networks to dynamical arrest in glass-forming liquids. Unlike ordinary ($k=1$) and biconnected ($k=2$) percolation, the mean field $k\geqslant 3$-core percolation transition is both continuous *and* discontinuous, i.e., there is a jump in the order parameter accompanied with a diverging length scale. To determine whether or not this hybrid transition survives in finite dimensions, we present a $1/d$ expansion for k-core percolation on the d-dimensional hypercubic lattice. We show that to order $1/d^3$ the singularity in the order parameter and in the susceptibility occur at the same value of the occupation probability. This result suggests that the unusual hybrid nature of the mean field k-core transition survives in high dimensions.

DOI: 10.1103/PhysRevE.72.046123 PACS number(s): 64.60.Ak

I. INTRODUCTION

In a number of physical problems long-range order requires more than a single stranded path to propagate over long distances. One example of this is the propagation of quadrupolar order in solid $(\text{ortho-}H_2)_x(\text{para-}H_2)_{1-x}$ mixtures [1]. This system can be reasonably modeled as a quenched, site-diluted lattice of electrostatic quadrupoles interacting via nearest-neighbor interactions on a fcc lattice. Since the lowest state of two such quadrupoles at displacement $\mathbf{r}$ is one in which one molecule may assume any orientation in the plane perpendicular to $\mathbf{r}$, it is clear that long-range order cannot propagate down a long noncollinear single stranded path. Therefore, to develop long-range order quadrupoles in an "infinite cluster" must have more than two nearest-neighboring quadrupoles.

Another such example of multipath long-range ordering is rigidity percolation [2–6] where each occupied site on a lattice has g degrees of freedom. The degrees of freedom of the site become fixed as more neighboring sites become occupied—one occupied neighbor constrains one degree of freedom. Therefore, in order to participate in the infinite rigid cluster, an occupied site must have at least g occupied neighbors. Here, again, is an example of a constraint on the minimum number of occupied neighbors giving rise to multiple long-range paths through the system.

More recently, an analogy between multipath percolation and the onset of elasticity in repulsive soft spheres as the packing fraction of the system is increased has been put forth by Schwarz *et al.* [7] (SLC). In the analogy overlaps between particles correspond to occupied neighboring sites. To ensure local mechanical stability for each particle, $d+1$ occupied neighbors are required for each occupied site, otherwise the site is unstable and it is removed from the system (as opposed to running into other particles in the system). Here, the $d+1$ constraint gives rise to multiply connected paths that eventually span the system. The onset of elasticity in the repulsive soft sphere system—a type of jamming transition called point J—is thought to have implications for other phenomena such as the glass transition and the colloidal glass transition [8,9].

The particular model of percolation called k-core, or bootstrap, percolation [7,10,11] turns out to be the relevant model of interest for such systems. For both the solid ortho-para H_2 mixtures and the jamming system, k-core percolation is an approximate description. However, for rigidity percolation, at least on the Bethe lattice, g-rigidity percolation is equivalent to $(g+1)$-core percolation [12]. In k-core percolation, each bond is independently occupied with probability p and vacant with probability $1-p$. In addition, it is required that sites with less than k occupied neighbors should be made vacant. This "culling" operation proceeds recursively until *all* remaining unculled occupied sites have at least k neighbors, as illustrated in Fig. 1 for a Bethe lattice where each site has z neighbors with $z=4$. Such a model gives rise to "many" paths emanating to infinity from a single site for large enough p.

Analysis of k-core percolation on the Bethe lattice by SLC showed that the critical point has some unusual characteristics. As was known previously [10], they found that the transition at $p=p_0$—the p at which an infinite cluster appears—is a discontinuous one for $k\geqslant 3$, and the probability P_∞ that a site be in the infinite cluster (after culling) exhibits the power law behavior:

$$P_\infty = \begin{cases} 0, & p < p_0, \\ P + a(p-p_0)^{1/2}, & p \geqslant p_0. \end{cases} \tag{1}$$

This result is to be contrasted with $k=1$ single stranded percolation where $P_\infty \sim (p-p_0)$ for $p\geqslant p_0$ [13]. More strikingly, SLC found a diverging correlation length and that an appropriate susceptibility has a power law divergence at the same threshold value of p at which the order parameter has a discontinuity.

An immediate question then arises, is this unusual structure of the critical point characteristic of infinite d, or does it survive for finite d? A clear answer to this question could be provided if a field theoretical formulation of the problem

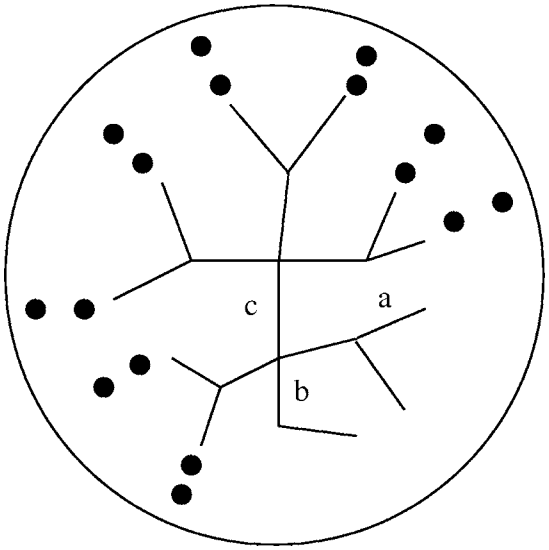

FIG. 1. Culling of a cluster for $k=3$ on a Bethe lattice with coordination number $z=4$. The filled circles indicate branches which are $k-1$ connected to infinity. Culling removes the bonds at a, b, and eventually at c, including the lower two sets of filled circles, but the rest of the cluster survives.

were available, but at present, no such field theory exists. (Although a field theory for the jamming transition based on force balance, as opposed to local mechanical stability, has been recently proposed [14], it is not obvious that this model is in the same universality class as k-core percolation in finite dimensions.) As for lattice models in low d spatial dimensions, until recently, numerical studies indicate that the k-core transition is *either* continuous or $p_c=1$, i.e., nothing survives the culling process until the lattice is fully occupied [15,16]. A case of the former is $k=3$ on the triangular lattice [17], and for the latter, $k=3$ on the square lattice [15]. In fact, for $k=3$ on the square lattice it has been proven by van Enter [18] that $p_c=1$ [19]. Moreover, it has recently been proven for hypercubic lattices that $p_c=1$ for $k \geqslant d+1$ [20]. To date, the only numerical evidence for a k-core transition with a jump in the order parameter and yet a diverging correlation length is a k-core-like model in two dimensions studied by SLC [21]. This result supports the notion that the unusual nature of the k-core transition found in the mean field survives in finite dimensions, though simple lattices, like the square lattice, are probably not the place to look for such a transition.

Lacking a k-core field theory and the sparsity of finite d numerical results, we decided to implement an expansion in $1/d$. As one sees for the Ising model, this expansion cannot be used to discuss critical exponents, because these exponents are independent of d for $d>d_c$, where d_c is the so-called upper critical dimension. For the Ising model, $d_c=4$ [22,23] and for ordinary percolation is $d_c=6$ [24,25]. However, this expansion has been used to generate short series in $1/d$ for the critical value of the coupling constant in problems such as the Ising model and self-avoiding walks [26], for spin glasses [27], for lattice animals [28], and for ordinary percolation [29]. Thus, this expansion is ideally suited to answer the question or whether or not the unusual k-core

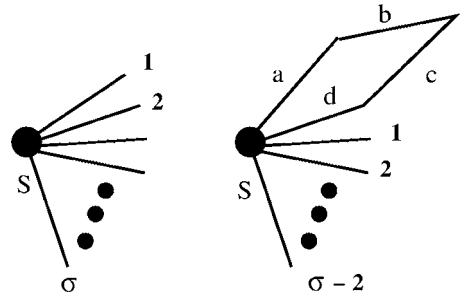

FIG. 2. Diagrammatic representation of the EOS. Left: the unperturbed EOS based on a seed site, S, with σ emerging bonds. Right: the perturbation to the EOS from the insertion of a square, so that now the seed site has $\sigma-2$ single bonds and an attached square.

mean field transition survives in finite dimensions. It should also be noted that the interpolation to continuous dimension implied by this expansion is precisely the same [30] as that used by Wilson in his development of the renormalization group [22]. We will use this expansion to calculate corrections up to order d^{-3} for the critical coupling constant at which the discontinuity in the order parameter takes place and compare it to the critical value at which the susceptibility diverges. Since we find that these two threshold remain equal up to this order in $1/d$, we conclude that it is likely that this coincidence is robust and remains true at least for some range of high d. We note that these results are stronger than the results of Toninelli *et al.* [20] showing that the unusual nature of the transition survives on Husimi trees (a Bethe lattice with finite loops), since, like the Bethe lattice, this structure has an infinite fractal dimension and therefore provides no information on the situation for finite d.

Briefly this paper is organized as follows. In Sec. II we review known results for the Bethe lattice to fix our notation. Section III introduces the notion of perturbing the equation of state. Section IV introduces the concepts behind the $1/d$ expansion. Section V presents the perturbative $1/d$ corrections to the equation of state, while Sec. VI does the same for the susceptibility. In Sec. VII we summarize the conclusions which may be drawn from our result, that to order $1/d^3$ at large d, the k-core transition remains a hybrid transition and in Sec. VIII we discuss implications of our result for systems such as glass-forming liquids.

II. BETHE LATTICE EQUATION OF STATE

In this section we construct the self-consistent equation for the order parameter on the Bethe lattice for k-core bond percolation. For this purpose we consider a rooted Bethe lattice, i.e., a lattice emanating from a seed site (as in Fig. 2) in which the lattice is constructed by recursively adding $\sigma \equiv z-1$ sites to each bond. To construct the self-consistent equation, the missing zth neighbor of the seed site is posited to survive culling. Therefore, the entire cluster will survive culling if each recursively added site has $k-1$ outward bond connections to infinity. We therefore define the quantity P_∞ to be the probability that when we add a site to the cluster, that site is then has $k-1$ outward bond connections to infinity which survive culling. The probability that some site on a

Bethe lattice is in the k-core can then be related to and has the same type of singular behavior as P_∞ for $k \geqslant 3$ [7]. Accordingly, we have the self-consistent equation of P_∞ as [7,10]

$$P_\infty = 1 - \sum_{m=0}^{m=k-2} \frac{\sigma!}{(\sigma-m)!m!}(1-pP_\infty)^{\sigma-m}(pP_\infty)^m, \quad (2)$$

which we write in terms of $Q \equiv pP_\infty$ as

$$Q/p = 1 - \sum_{m=0}^{m=k-2} \frac{\sigma!}{(\sigma-m)!m!}Q^m(1-Q)^{\sigma-m} \equiv \Phi(Q). \quad (3)$$

Starting at $p=1$, so that $Q=1$, we consider the effect of reducing p and find that

$$\frac{dQ}{dp} = (Q/p^2)\left[\frac{1}{p} - \frac{d\Phi}{dQ}\right]^{-1}. \quad (4)$$

As p is decreased, Q decreases until p reaches a critical value p_c at which

$$\frac{1}{p} = \frac{d\Phi(Q)}{dQ} = \frac{(\sigma-k+1)!}{(\sigma-k+1)!(k-3)!}Q^{k-2}(1-Q)^{\sigma-k+1}. \quad (5)$$

Indeed, when the description of the transition is phrased in this way, it seems almost obvious that "turning on" finite spatial dimension will not invalidate Eq. (1).

III. PERTURBATIVE CORRECTIONS TO $\Phi(Q)$

Now we wish to perturb the equation of state (EOS). For instance, we may consider what terms appear in the expansion of the EOS which depend on the variables $p_a p_b p_c p_d$, where a, b, c, and d form a square. We will construct

$$\Delta\Phi = \Phi_H - \Phi_B, \quad (6)$$

where the subscript on Φ indicates whether it is to be evaluated for the hypercubic (H) lattice or the Bethe (B) lattice. This expression includes the additional iterative term [which we only invoke once at order $1/\sigma^2$ where σ is $O(d)$] for the H lattice and it also takes account of terms which appear on the B lattice but which do not have counterparts on the H lattice.

To evaluate the derivative with respect to the p's in this expansion, we note that each occupied bond carries a factor of p and each unoccupied bond carries a factor of $1-p$. So for any bare diagram of b bonds, the derivative with respect to all its p's will involve a sum of the 2^b configurations of occupied and unoccupied bonds, in which an occupied bond carries a factor +1 and an unoccupied bond carries a factor −1. Thus, from a square (which is the configuration giving the leading correction at relative order $1/\sigma^2$) we generate 16 subdiagrams (the first of which is just the one for which all bonds are occupied and the last of which is the one for which all bonds are unoccupied). Accordingly, the derivative with respect to the four p's which form a square (the leading correction to the B lattice) gives rise to Figs. 3 for the H lattice and to Figs. 4–6 for the B lattice.

If $f(x)$ denotes the contribution to $\Delta\Phi$ from square insertions, which we call Φ_{sq}, then

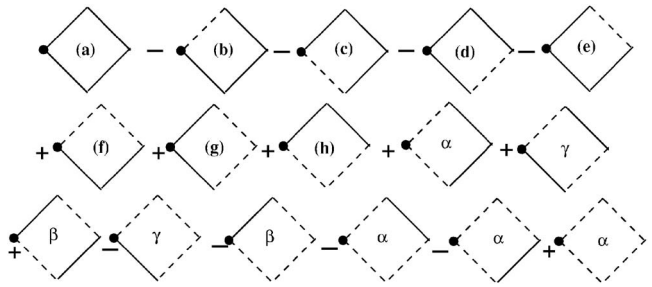

FIG. 3. Contributions from the 16 subdiagrams [of diagram (a)] which result from either occupying (full line) or not occupying (dashed line) each bond of the square on the H lattice. Greek letters label sets of subdiagrams which cancel one another.

$$\Phi_{sq} = f(a) - 2f(b) - 2f(d) - 2f(i) + 2f(j) + 2f(k) - f(m) + 2f(n) - 2f(q) + 2f(r), \quad (7)$$

where we noted that $f(f)=f(h)=f(l)$ and $f(g)=f(p)$. This equation is represented in Fig. 7. The factors of 2 take account of the fact that some topologies occur in two equivalent realizations. When we calculate the contributions f we must include not only the factor $p_a p_b p_c p_d = p^4$, but also the number of ways (which depends on σ) the bonds making up the square can be selected out of the σ available bonds. Since this factor is of order σ^2, we see that Φ_{sq} is of order $p^4\sigma^2$ which we will see is of order σ^{-2}. As will also be seen later, if we were only evaluating these corrections to leading order in $1/\sigma$, then we would not need to differentiate between diagrams (b), (j), and (r), or between (d), (k), and (n). Accordingly, at order $1/\sigma^3$, when we consider the analogous contribution from hexagons, Φ_{hex}, we do not have to be explicit about the configuration of the vacant bond(s) and we therefore have the hexagon insertions shown in Fig. 8.

Percolation

We can apply the above formulation to calculate the corrections to the critical concentration p_c in the ordinary bond percolation problem, and check the results by comparing to those obtained by Gaunt and Ruskin [29]. For percolation, a diagram contributes to the probability of the seed being connected to infinity if one or more of its vertices is connected to infinity. So, for the rooted Bethe lattice the EOS at the transition is

$$P = 1 - (1-pP)^\sigma. \quad (8)$$

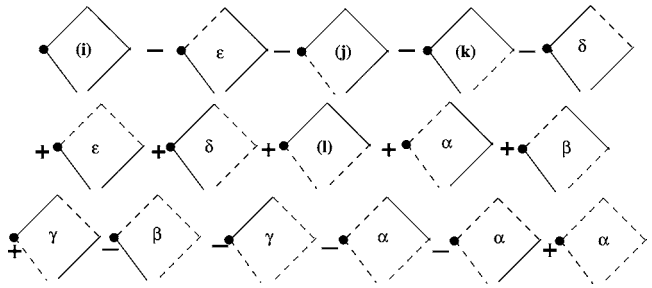

FIG. 4. As above, but for the B lattice. Vertices which are close to one another would coincide on the H lattice.

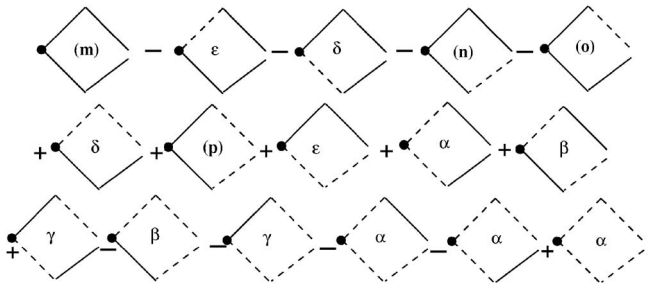

FIG. 5. As above, but for the B lattice.

(The only nonpercolating case is if all vertices are *not* connected to infinity.) Since the percolation transition is continuous, the critical concentration is found by expanding the EOS in powers of P. At linear order the solution requires that

$$1 = \sigma p_c. \tag{9}$$

For hypercubic lattices the contribution to $\Phi_{\rm sq}$ from Eq. (7) is written as

$$\begin{aligned}\Phi_{\rm sq} = \frac{1}{2}(\sigma-1)^2 p^4 \{&[1-(1-pP)^{\sigma-2}(1-P^{\sigma-1})^3] \\ &- 2[1-(1-pP)^{\sigma-2}(1-P^{\sigma-1})^3] - 2[1-(1-pP)^{\sigma-2} \\ &\times(1-P^{\sigma-1})^3] - 2[1-(1-P)^2(1-pP)^{\sigma-2}(1-P^{\sigma-1})^2] \\ &+ 2[1-(1-P)(1-pP)^{\sigma-2}(1-P^{\sigma-1})^2] + 2[1-(1-P) \\ &\times(1-pP)^{\sigma-2}(1-P^{\sigma-1})^2] - [1-(1-P)^2(1-pP)^{\sigma-2} \\ &\times(1-P^{\sigma-1})^2] + 2[1-(1-P)(1-pP)^{\sigma-2}(1-P^{\sigma-1})^2] \\ &- 2[1-(1-P)(1-pP)^{\sigma-1}(1-P^{\sigma-1})^3] \\ &+ 2[1-(1-pP)^{\sigma-1}(1-P^{\sigma-1})^3]\},\end{aligned} \tag{10}$$

where the terms in square brackets denote diagrams (a), (b), (d), etc. from Fig. 7, and

$$P^{\sigma-1} = 1-(1-pP)^{\sigma-1} + O(\sigma^{-2}). \tag{11}$$

$P^{\sigma-1}$ is the probability that a site has at least $k-1$ connections to infinity out of $\sigma-1$ bonds attached to the site. A generalization of this quantity will be introduced later on. $\Phi_{\rm sq}$ can be simplified to read

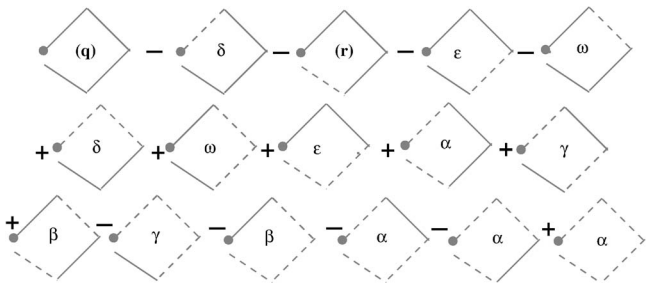

FIG. 6. As above, but for the B lattice.

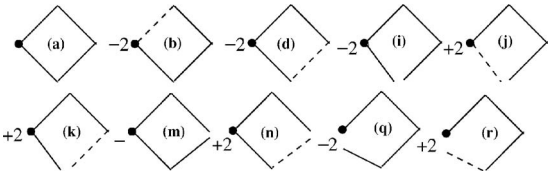

FIG. 7. Diagrammatic representation of Eq. (7). Note that there are no diagrams with two unoccupied bonds. This is because for every H lattice diagram there is a B lattice equivalent with a "cut" between the two unoccupied bonds resulting in a cancellation.

$$\begin{aligned}\Phi_{\rm sq} = \frac{1}{2}(\sigma-1)^2 p^4 [&-2P(1-pP)^{\sigma-1}(1-P^{\sigma-1})^3 + 3(1 \\ &- pP)^{\sigma-2}(1-P^{\sigma-1})^3 + 3(1-pP)^{\sigma-2}(1-P^{\sigma-1})^2(1-P)^2 \\ &- 6(1-pP)^{\sigma-2}(1-P^{\sigma-1})^2(1-P)].\end{aligned} \tag{12}$$

The factors of $(1-pP)^{\sigma-2}$ and $(1-pP)^{\sigma-1}$ ensure that the bonds attached to the seed site but not in the square are isolated from infinity, and the factor $N_{\rm sq}=(\sigma-1)^2/2$ counts the number of possible squares. We construct $N_{\rm sq}$ using Fig. 9 as follows. Say the bond to which we wish to attach the square is in the x_1 direction. Then there are two cases: either the square involves a bond in x_1 direction or it does not. In the first case the square involves the x_1 bond and one of $2d-2=\sigma-1$ choices for the other axis of the square. The x_1 bond can be either the first or the second leg of the square, but we ignore this degeneracy because it simply corresponds to traversing the square in different senses. So for this case there are $(\sigma-1)$ configurations. In the second case the square involves two out of $d-1$ dimensions, so there are $4(d-1)\times(d-2)/2=(\sigma-1)(\sigma-3)/2$ such configurations. In all

$$N_{\rm sq} = (\sigma-1)^2/2. \tag{13}$$

This number would be twice as large if the sense in which the square was traversed mattered. For hexagons the calculation is much simpler because we do not need to keep track of the configuration of vacant bonds, which forces us to distinguish between P and $P^{\sigma-1}$ and which leads to corrections of relative order $1/\sigma$. Using Fig. 8, we write the contribution to $\Delta\Phi$ from hexagons in leading order of $1/\sigma$ as

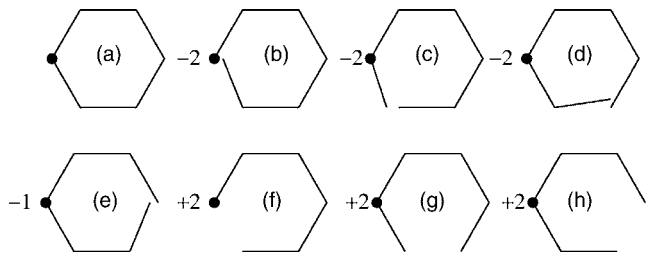

FIG. 8. As in Fig. 7, contributions to $\Phi(Q)$ from hexagons on either a H or a B lattice. Diagrams (f), (g), and (h) correspond to sums of graphs on both the H and B lattices. For example, the square equivalent to hexagon diagram (f) is the sum of diagrams (b), (r), and (j) in Fig. 7. Diagrams similar to these give the contribution to the susceptibility, $\Gamma_{H,A}$, due to hexagon insertions as we will eventually show.

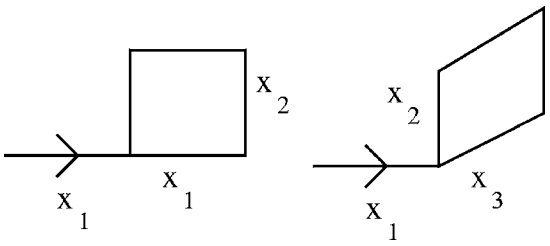

FIG. 9. Attaching a square to a site.

$$\Delta\Phi_{\rm hex} = -2\sigma^3 p^6 (1-pP)^{\sigma-2}\{5(1-P)^5(1-[1-P]) + 2(1-pP)(1-P)^5(1-[1-P])\} = -2\sigma^3 p^6 (1-pP)^{\sigma-2} P(1-P)^5[5+2(1-pP)]. \quad (14)$$

Here the factor $2\sigma^3$ is (to leading order in $1/\sigma$) the number of ways of attaching a hexagon to a site. Note that $p \to 1/\sigma + O(\sigma^{-3})$ so that to the order we need, $P^{\sigma-1} \sim P[1-(1/\sigma)]$. Also note that for this continuous transition we only need the contribution to $\Delta\Phi$ which are linear in P. Thus we set $\Delta\Phi_{\rm hex} = -14P\sigma^{-3}$ and then

$$\Delta\Phi = -\frac{P}{2\sigma^2}\left(1-\frac{1}{\sigma}\right)^2\{2+3[1-(1/\sigma)]\} - 14\frac{P}{\sigma^3}. \quad (15)$$

Finally, using $1 = \sigma p_c + d\Delta\Phi/dP$, we get

$$\sigma p_c = 1 + (5/2)\sigma^{-2} + (15/2)\sigma^{-3} + O(\sigma^{-4}), \quad (16)$$

in agreement with Ref. [29].

IV. EXPANSION IN POWERS OF $1/\sigma$

Before getting into the calculation we should indicate how the various variables are to be expanded in powers of $1/\sigma$. Consider Eqs. (3) and (5). Set

$$p_0 = \sum_n \beta_n \sigma^{-n}, \quad Q_0 = \sum_n \alpha_n \sigma^{-n}, \quad (17)$$

where the subscripts "0" indicate that the quantities are those of the Bethe lattice solution. Although we will not invoke the actual values of the coefficients in these expansions, we will, for illustrative purposes, determine the leading coefficients $\alpha_1 \equiv \alpha$ and $\beta_1 \equiv \beta$, where

$$\frac{\alpha}{\beta} = 1 - e^{-\alpha}\sum_{m=0}^{m=k-2}\frac{\alpha^m}{m!} \quad (18)$$

and

$$1 = \beta\alpha^{k-2}e^{-\alpha}. \quad (19)$$

By eliminating β, we obtain an equation which determines α:

$$e^{\alpha} = \alpha^{k-1} + \sum_{m=0}^{m=k-2}\frac{\alpha^m}{m!}. \quad (20)$$

For $k=3$, numerical evaluation yields the approximate values $\alpha = 1.793\,282\,133$ and $\beta = 3.350\,918\,872$. As we shall see, it is more convenient to express results in terms of p_0 and Q_0 because our main aim is not to explicitly obtain an expansion for these quantities in powers of $1/\sigma$, but rather to determine whether or not the singularity in the EOS state coincides with the singularity in the susceptibility.

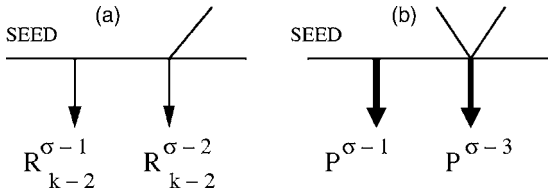

FIG. 10. Definition of $R_k^{\sigma-m}$ (a) and $P^{\sigma-r}$ (b). Each site has $\sigma+1$ bonds.

Now we see how the critical coupling constants $p_c(d), Q_c(d)$ for hypercubic lattices are obtained after $\Delta\Phi$ has been evaluated. We write

$$\frac{Q}{p} = \Phi_0(Q) + \Delta\Phi(Q,p), \quad \frac{1}{p} = \frac{d\Phi_0}{dQ} + \frac{d\Delta\Phi(Q,p)}{dQ}, \quad (21)$$

and set

$$p = p_0 + \Delta p, \quad Q = Q_0 + \Delta Q. \quad (22)$$

In this analysis we note that $\Delta\Phi \sim \sigma^{-2}$, so that to obtain results to order σ^{-3} we need only consider terms linear in $\Delta\Phi$, Δp, or ΔQ. Then we have

$$\frac{Q_0}{p_0} + \frac{\Delta Q}{p_0} - \frac{Q_0\Delta p}{p_0^2} = \Phi_0(Q_0) + \Delta Q\frac{d\Phi_0(Q_0)}{dQ} + \Delta\Phi(Q_0,p_0), \quad (23)$$

which gives

$$\Delta p = -\frac{p_0^2}{Q_0}\Delta\Phi(Q_0,p_0). \quad (24)$$

Also

$$\frac{1}{p_0} - \frac{\Delta p}{p_0^2} = \frac{d\Phi_0(Q_0)}{dQ} + \Delta Q\frac{d^2\Phi_0}{dQ^2} + \frac{d\Delta\Phi(Q_0,p_0)}{dQ}, \quad (25)$$

which gives

$$\Delta Q = \left(\frac{d^2\Phi_0}{dQ^2}\right)^{-1}\left(-\frac{\Delta p}{p_0^2} - \frac{d\Delta\Phi}{dQ}\right) = \left(\frac{d^2\Phi_0}{dQ^2}\right)^{-1}\left(\frac{\Delta\Phi(Q_0,p_0)}{Q_0} - \frac{d\Delta\Phi}{dQ}\right). \quad (26)$$

We introduce the following Bethe lattice quantities. First, $R_r^{\sigma-m}$ is defined to be the probability that out of $\sigma-m$ available bonds, exactly r are $k-1$ connected outward (i.e. away from the origin or seed of the cluster) to infinity and we set $R_r^{\sigma-1} \equiv R_r$. (It is also convenient to set $R_{k-2} \equiv R$.) This definition of R is illustrated in Fig. 10. Similarly we define $P^{\sigma-m}$ to be the probability that a site is *at least* $k-1$ connected to infinity through the set of $\sigma-m$ of bonds and $P^{\sigma} \equiv P$. Since Q is of order $1/\sigma$, we see that $P^{\sigma-m}$ is of order $1/\sigma^0$ (assuming m is of order unity). One can likewise show that under this same assumption $R_r^{\sigma-m}$ is also of order unity. Note when

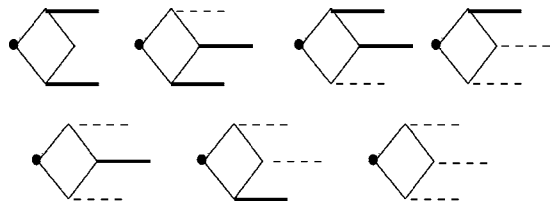

FIG. 11. Configurations of diagram (a) of Fig. 7 which have two paths to infinity. The heavy line is a bond which is $(k-1)$-connected to infinity and carries a factor $P^{\sigma-1}$. The dashed line carries a factor R_{k-2} which may survive culling if it is connected to two live bonds.

the superscript on P is of the form $\sigma-n$ then the superscript indicates the number of bonds, as defined above. When the superscript is a purely numerical value like 2, then this indicates an exponent: $P^2=P\times P$.

We now express all the above Bethe lattice quantities in terms of the canonical variables R, P, and $Q_0\equiv p_0P$. We have

$$P^{\sigma-r}=1-\sum_{m=0}^{m=k-2}\frac{(\sigma-r)!}{(\sigma-r-m)!m!}Q_0^m(1-Q_0)^{\sigma-r-m}, \quad (27)$$

from which we obtain, correct to first order in $1/\sigma$, that

$$P^{\sigma-r}=P-rQ_0R+O(\sigma^{-2}). \quad (28)$$

Also,

$$R_m^{\sigma-1-r}=Q_0^m\frac{(\sigma-1-r)!}{m!(\sigma-1-r-m)!}(1-Q_0)^{\sigma-1-r-m} \quad (29)$$

$$=R_m\left(1+rQ_0-\frac{rm}{\sigma}\right)+O(\sigma^{-2}), \quad (30)$$

$$\frac{dP}{dQ}=\sigma R, \quad (31)$$

and

$$\begin{aligned}\frac{dR_m}{dQ}&=\frac{(\sigma-1)!}{(m-1)!(\sigma-m-1)!}Q_0^{m-1}(1-Q_0)^{\sigma-m-1}\\&\quad-\frac{(\sigma-1)!}{m!(\sigma-m-2)!}Q_0^m(1-Q_0)^{\sigma-m-2}\\&=\frac{1}{1-Q_0}\left(\frac{(\sigma-1)!}{(m-1)!(\sigma-m-1)!}Q_0^{m-1}(1-Q_0)^{\sigma-m}\right.\\&\quad\left.-\frac{(\sigma-1)!}{m!(\sigma-m-2)!}Q_0^m(1-Q_0)^{\sigma-m-1}\right)\\&=\frac{1}{1-Q_0}((\sigma-m)R_{m-1}-(\sigma-m-1)R_m)=(\sigma-m+Q)\\&\quad\times(R_{m-1}-R_m)+R_m+O(1/\sigma). \quad (32)\end{aligned}$$

V. $1/\sigma$ EXPANSION FOR THE EQUATION OF STATE

In this section we will implement the $1/\sigma$ expansion for the EOS. Note that we are considering the effect of having a

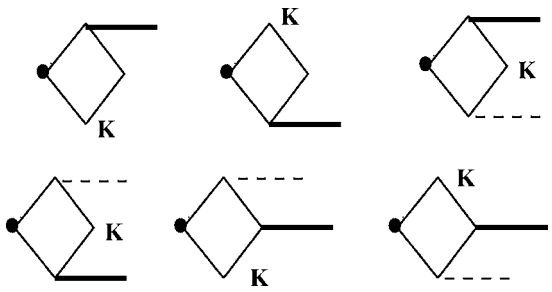

FIG. 12. As in Fig. 11, configurations of diagram (a) of Fig. 7 which have one path to infinity. The symbol K denotes a bond which is definitely culled and therefore carries a factor $(1-P^{\sigma-1}-R_{k-2})$.

square (or hexagon) of bonds with one vertex at the seed site (Fig. 2). All structures emanating from this square (or hexagon) or from the other $\sigma-2$ bonds which intersect the seed site, may be assumed to be treelike because the occurrence of more than one loop only influences terms of relative order $1/\sigma^4$ and we do not consider this order. Accordingly we implement Eq. (7). For squares we have $f(n)=[(\sigma-1)^2p^4/2]\delta f(n)$, where n indicates the diagram as labeled in Eq. (7). Since the insertion of the square (or hexagon) can contribute a maximum of two more paths to the boundary (or infinity) at the seed site, we will break up diagram (a) of Fig. 7 into factors associated with having two, one, and zero paths to infinity as illustrated in Figs. 11–13, respectively. Thereby we find

$$\begin{aligned}\delta f(a)&=(R_{k-3}^{\sigma-2}+R_{k-2}^{\sigma-2}+P^{\sigma-2})[(P^{\sigma-1})^2+2R(P^{\sigma-1})^2+3R^2P^{\sigma-1}\\&\quad+R^3]+(R_{k-2}^{\sigma-2}+P^{\sigma-2})(2+4R)P^{\sigma-1}(1-P^{\sigma-1}-R)\\&\quad+P^{\sigma-2}[(1-P^{\sigma-1}-R)^2+2R(1-P^{\sigma-1}-R)^2+3R^2(1\\&\quad-P^{\sigma-1}-R)]\\&=R_{k-3}^{\sigma-2}[(P^{\sigma-1})^2+2R(P^{\sigma-1})^2+3R^2P^{\sigma-1}+R^3]+R_{k-2}^{\sigma-2}\\&\quad+P^{\sigma-2}-R_{k-2}^{\sigma-2}[(1-P^{\sigma-1}-R)^2+2R(1-P^{\sigma-1}-R)^2\\&\quad+3R^2(1-P^{\sigma-1}-R)]. \quad (33)\end{aligned}$$

In constructing this expression we noted that if the square had two paths to infinity, then the remaining $\sigma-2$ bonds emanating from the seed site had to have at least $k-3$ paths to infinity which we take into account with the factor of the form $R_{k-3}+R_{k-2}+P$. (P is the probability of having at least $k-1$ paths to infinity.) The factor $R_{k-2}+P$ and P take account of having at least $k-2$ or $k-1$ paths to infinity, respectively.

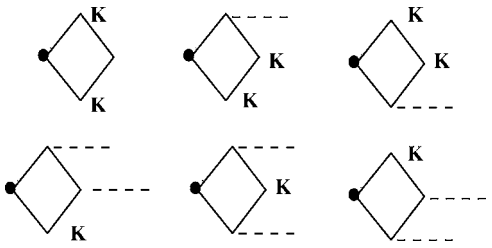

FIG. 13. As in Figs. 11 and 12 configurations of diagram (a) of Fig. 7 which have no paths to infinity.

Similarly, for the other diagrams of 7 we have

$$\delta f(b) = (P^{\sigma-2} + R_{k-2}^{\sigma-2})P^{\sigma-1}(1 + R + R^2) + P^{\sigma-2}[1 - P^{\sigma-1}(1 + R + R^2)] = P^{\sigma-2} + R_{k-2}^{\sigma-2}P^{\sigma-1}(1 + R + R^2), \quad (34)$$

$$\delta f(d) = (P^{\sigma-2} + R_{k-2}^{\sigma-2} + R_{k-3}^{\sigma-2})(P^{\sigma-1})^2(1 + R) + (P^{\sigma-2} + R_{k-2}^{\sigma-2}) \times \{P^{\sigma-1}[1 - P^{\sigma-1}(1 + R)] + (1 - P^{\sigma-1})P^{\sigma-1}(1 + R)\} + P^{\sigma-2}(1 - P^{\sigma-1})[1 - P^{\sigma-1}(1 + R)] = P^{\sigma-2} + R_{k-2}^{\sigma-2} + R_{k-3}^{\sigma-2}(P^{\sigma-1})^2(1 + R) - R_{k-2}^{\sigma-2}(1 - P^{\sigma-1})[1 - P^{\sigma-1}(1 + R)], \quad (35)$$

$$\delta f(i) = P^{\sigma-2}(1 - P)[1 - P_{\infty}^{\sigma-1}(1 + R) - PR^2] + (R_{k-2}^{\sigma-2} + P^{\sigma-2}) \times \{(1 - P)[P^{\sigma-1}(1 + R) + PR^2] + P[1 - P_{\infty}^{\sigma-1}(1 + R) - PR^2)]\} + (R_{k-3}^{\sigma-2} + R_{k-2}^{\sigma-2} + P^{\sigma-2})P[P^{\sigma-1}(1 + R) + PR^2] = R_{k-2}^{\sigma-2} + P^{\sigma-2} + R_{k-3}^{\sigma-2}P[P^{\sigma-1}(1 + R) + PR^2] - R_{k-2}^{\sigma-2}(1 - P)[1 - P^{\sigma-1}(1 + R) - PR^2], \quad (36)$$

$$\delta f(j) = (P^{\sigma-2} + R_{k-2}^{\sigma-2})[P^{\sigma-1}(1 + R) + PR^2] + P^{\sigma-2}[1 - P^{\sigma-1}(1 + R) - PR^2] = P^{\sigma-2} + R_{k-2}^{\sigma-2}[P^{\sigma-1}(1 + R) + PR^2], \quad (37)$$

$$\delta f(k) = (P^{\sigma-2} + R_{k-2}^{\sigma-2} + R_{k-3}^{\sigma-2})PP^{\sigma-1}(1 + R) + (P^{\sigma-2} + R_{k-2}^{\sigma-2}) \times \{P^{\sigma-1}[1 - P](1 + R) + P[1 - P^{\sigma-1}(1 + R)\} + P^{\sigma-2}(1 - P)[1 - P^{\sigma-1}(1 + R)] = P^{\sigma-2} + R_{k-2}^{\sigma-2} + R_{k-3}^{\sigma-2}PP^{\sigma-1}(1 + R) - R_{k-2}^{\sigma-2}(1 - P)[1 - P^{\sigma-1}(1 + R)], \quad (38)$$

$$\delta f(m) = P^{\sigma-2}(1 - P^{\sigma-1} - RP)^2 + 2(P^{\sigma-2} + R_{k-2}^{\sigma-2})(1 - P^{\sigma-1} - RP)(P^{\sigma-1} + RP) + (R_{k-3}^{\sigma-2} + R_{k-2}^{\sigma-2} + P^{\sigma-2})(P^{\sigma-1} + RP)^2 = P^{\sigma-2} + R_{k-2}^{\sigma-2} + R_{k-3}^{\sigma-2}(P^{\sigma-1} + RP)^2 - R_{k-2}^{\sigma-2}(1 - P^{\sigma-1} - RP)^2, \quad (39)$$

$$\delta f(n) = P^{\sigma-2} + R_{k-2}^{\sigma-2} + R_{k-3}^{\sigma-2}P^{\sigma-1}[P^{\sigma-1} + RP] - R_{k-2}^{\sigma-2}(1 - P^{\sigma-1}) \times (1 - P^{\sigma-1} - PR), \quad (40)$$

$$\delta f(q) = P^{\sigma-1}[1 - P^{\sigma-1}(1 + R + R^2) - R^3P] + (R + P^{\sigma-1})[P^{\sigma-1} + R^2(1 + R) + R^3P] = P^{\sigma-1} + R[P^{\sigma-1}(1 + R + R^2) + R^3P], \quad (41)$$

$$\delta f(r) = (P^{\sigma-1} + R)P^{\sigma-1}(1 + R + R^2) + P^{\sigma-1}[1 - P^{\sigma-1}(1 + R + R^2)] = P^{\sigma-1} + RP^{\sigma-1}(1 + R + R^2). \quad (42)$$

With these results we are now ready to evaluate Eq. (7) and it reads

$$\Phi_{\mathrm{sq}} = \frac{(\sigma-1)^2p^4}{2}[R_{k-3}^{\sigma-2}(R^3 + 3R^2P^{\sigma-1} - 3R^2P^2) - 2R^4P + R_{k-2}^{\sigma-2}(R^3 - 3R^2P^{\sigma-1} + 3R^2P^2)]. \quad (43)$$

Since the contributions from hexagons only need to be evaluated to leading order in $1/\sigma$, the configuration of vacant bonds is irrelevant and we may omit the superscripts on R and P. Accordingly, for hexagons it is convenient to classify (as indicated by the subscript) the value of m, the number of paths to infinity. For diagram x we write

$$f_m(x) = 2\sigma^3p^6\delta f_m(x), \quad (44)$$

where $2\sigma^3$ is the number of hexagons (to lowest order in $1/\sigma$) that can be attached to a bond and

$$\delta f_2(a) = P^2(1 + 2R + 3R^2 + 4R^3) + 5R^4P + R^5, \quad (45)$$

$$\delta f_1(a) = 2P(1 - P - R)(1 + 2R + 3R^2 + 4R^3), \quad (46)$$

$$\delta f_0(a) = (1 - P - R)^2(1 + 2R + 3R^2 + 4R^3) + 5R^4(1 - P - R), \quad (47)$$

$$\delta f_1(b) = P(1 + R + R^2 + R^3 + R^4 + R^5), \quad (48)$$

$$\delta f_0(b) = (1 - P - R)(1 + R + R^2 + R^3 + R^4) + R^5(1 - P), \quad (49)$$

$$\delta f_2(c) = P^2(1 + R + R^2 + R^3 + R^4), \quad (50)$$

$$\delta f_1(c) = (1 - P)P(1 + R + R^2 + R^3 + R^4) + P(1 - P - R)(1 + R + R^2 + R^3) + P(1 - P)R^4, \quad (51)$$

$$\delta f_0(c) = (1 - P)(1 - P - R)(1 + R + R^2 + R^3) + (1 - P)^2R^4, \quad (52)$$

$$\delta f_2(d) = P^2(1 + R + R^2 + R^3)(1 + R), \quad (53)$$

$$\delta f_1(d) = P(1 - P - RP)(1 + R + R^2 + R^3) + P(1 + R)[(1 - P - R)(1 + R + R^2) + (1 - P)R^3], \quad (54)$$

$$\delta f_0(d) = (1 - P - RP)[(1 - P - R)(1 + R + R^2) + (1 - P)R^3], \quad (55)$$

$$\delta f_2(e) = [P(1 + R + R^2)]^2, \quad (56)$$

$$\delta f_1(e) = 2P(1 + R + R^2)[(1 - P - R)(1 + R) + R^2(1 - P)], \quad (57)$$

$$\delta f_0(e) = [(1 - P - R)(1 + R) + R^2(1 - P)]^2, \quad (58)$$

$$\delta f_1(f) = P(1 + R + R^2 + R^3 + R^4), \quad (59)$$

$$\delta f_0(f) = [(1-P-R)(1+R+R^2+R^3)+(1-P)R^4], \tag{60}$$

$$\delta f_2(g) = P^2(1+R+R^2+R^3), \tag{61}$$

$$\delta f_1(g) = P(1-P)(1+R+R^2+R^3)+P[(1-P-R)(1+R+R^2)+(1-P)R^3], \tag{62}$$

$$\delta f_0(g) = (1-P)[(1+R+R^2)(1-P-R)+(1-P)R^3], \tag{63}$$

$$\delta f_2(h) = P^2(1+R+R^2)(1+R), \tag{64}$$

$$\delta f_1(h) = (1-P-RP)P(1+R+R^2)+P(1+R)(1-P-RP-R^2P), \tag{65}$$

$$\delta f_0(h) = (1-P-RP)(1-P-RP-R^2P), \tag{66}$$

where the numbering of contributions is as in Fig. 8. Thus for the contribution of hexagons to the EOS (indicated by the superscript H), the sum over diagrams gives

$$\Phi_2^H = f_2(a)-2f_2(c)-2f_2(d)-f_2(e)+2f_2(g)+2f_2(h) = 2\sigma^3p^6(-5R^4P_\infty^2+5R^4P_\infty+R^5), \tag{67}$$

$$\Phi_1^H = f_1(a)-2f_1(b)-2f_1(c)-2f_1(d)-f_1(e)+2f_1(f)+2f_1(g)+2f_1(h) = 2\sigma^3p^6[10R^4P_\infty^2-(10R^4+2R^5)P_\infty], \tag{68}$$

and

$$\Phi_0^H = f_0(a)-2f_0(b)-2f_0(c)-2f_0(d)-f_0(e)+2f_0(f)+2f_0(g)+2f_0(h) = 2\sigma^3p^6[-5R^4P_\infty^2+(5R^4+2R^5)P_\infty-R^5]. \tag{69}$$

It is a check on our results that $\Sigma_n\Phi_n^H=0$. Now we match each of these contributions to possible configurations of the other $\sigma-2$ bonds from the seed site. Thus, from hexagons we get

$$\Phi_{\rm hex} = P\Phi_0^H+(P+R)\Phi_1^H+(P+R+R_{k-3})\Phi_2^H = R_{k-3}\Phi_2^H-R\Phi_0^H. \tag{70}$$

VI. $1/\sigma$ EXPANSION FOR THE SUSCEPTIBILITY

A. Formulation of the susceptibility

In this section we consider the $1/\sigma$ expansion for the two-point (i,j) susceptibility χ_{ij}. For k-core percolation we calculate this quantity in the ordered phase, because for the Bethe lattice there are no finite k-core clusters. Here we define $\chi=\Sigma_j\chi_{ij}$, where

$$\chi_{ij} = \langle \nu_i\nu_j\rangle - \langle\nu_i\rangle\langle\nu_j\rangle, \tag{71}$$

where ν_i is an indicator variable which is unity if the site i is in the k-core and is zero otherwise. Also the angle brackets indicate an average of configurations of bonds in which each bond is independently present with probability p and absent with probability $1-p$.

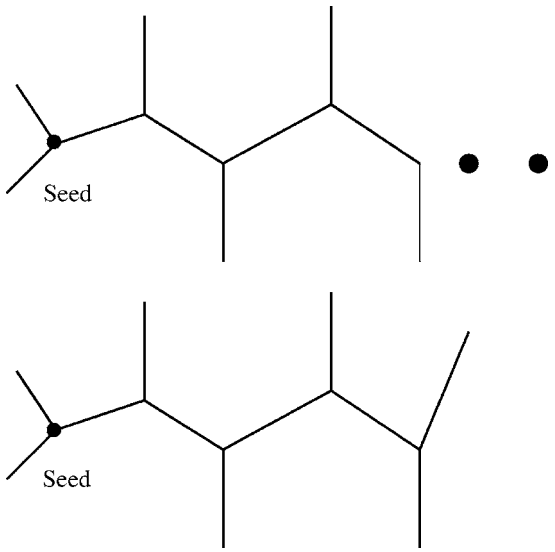

FIG. 14. Configurations for $k=3$ illustrating "truncation" of diagrams. Here the side branches are assumed to be $(k-1)$-connected to infinity. In the top panel a configuration is shown where the k–core depends on the state of the further bonds indicated by filled circles. In the lower panel, the configuration is $(k=3)$-connected no matter what happens further down the chain. Since the k–core does not depend on further bond occupation probabilities this diagram cannot be extended.

Now we formulate the $1/\sigma$ expansion for the ordered phase of k-core percolation. On the Bethe lattice the long-range part of this correlation function comes from the probability of configurations in which two sites are only in the k-core by virtue of the presence of a path of occupied bonds connecting sites i and j. (Of course each site on this path must belong to the k-core.) In this connection, it is important that the sites not be in the k- if any bond is removed. Such contributions are either already counted in lower order or are canceled when the second term in Eq. (71) is subtracted off. Thus the configuration in panel (a) of Fig. 14 is an allowed configuration contributing to χ_{ij}, but that in panel (b) can not be extended. In Ref. [7], this consideration led to equivalently restricting the sum to the "corona." Thus, as the path is progressively lengthened, if we reach a point where the origin of the path is certainly in the k-core no matter how the path is extended, then this path is said to be "truncated," and is discarded as not contributing to the singularity in χ.

For the present work we obtain the results of Ref. [7] as follows. For a path to satisfy the "corona" constraint, it must consist of a path for which each vertex is $k-2$ connected to infinity if the bonds along the path are not considered. With this construction one sees that at each vertex, whether the whole structure is or is not k-connected to infinity, depends on what happens further down the path. Thus, for the Bethe lattice each vertex in the path leading from site i to site j carries a factor $pR_{k-2}^{\sigma-1}=pR_{k-2}=pR$. When χ_{ij} is summed over j, one obtains a geometric series in the ratio, r, given by

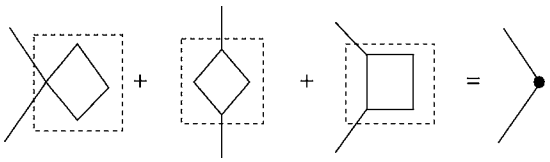

FIG. 15. The factors associated with the dashed box in the first three diagrams renormalize the vertex (the filled circle) in the last diagram. We label these contributions SQ1, SQ2, and SQ3, respectively.

$$r = \sigma p R_{k-2}, \tag{72}$$

which coincides with the singularity in the EOS [7].

A convenient way to describe the $1/\sigma$ expansion as applied to the susceptibility, is to regard the $1/\sigma$ corrections as a vertex correction, as illustrated in Fig. 15 for insertions of a square. This vertex correction amounts to replacing R_{k-2} by $R_{k-2}+\Delta R$, where ΔR is the contribution from the dashed box (which replaces each vertex). Analogous corrections arise at relative order $1/\sigma^3$ from insertions of hexagons. However, insertions involving two or more loops lead to corrections of order $1/\sigma^4$ and higher and are beyond the scope of the present calculation. [Note that for the last diagram, SQ3, we need an extra factor of 2 because the two sides of the square are inequivalent, so that it occurs $(\sigma-1)^2$ ways.] The diagrams for a square insertion into a chain diagram for the susceptibility are shown more explicitly below.

The condition for a divergent susceptibility is that the perturbed ratio r be unity, or

$$1 = r = \sigma p R + \sigma p \Delta R. \tag{73}$$

We now evaluate the ratio r at the singularity in the EOS, so that p and Q are given by Eqs. (22), (24), and (26). Working to leading order we write

$$\begin{aligned} r &= \sigma(p_0 + \Delta p)\left(R(Q_0) + \frac{dR}{dQ_0}\Delta Q\right) + \sigma p \Delta R \\ &= 1 + \frac{\Delta p}{p_0} + \frac{1}{R}\frac{dR}{dQ_0}\Delta Q + \sigma p_0 \Delta R \\ &= 1 - \frac{p_0}{Q_0}\Delta\Phi + \frac{1}{R}\frac{dR}{dQ_0}\left(\sigma\frac{dR}{dQ_0}\right)^{-1}\left(\frac{\Delta\Phi}{Q_0} - \frac{d\Delta\Phi}{dQ}\right) + \sigma p_\Delta R \\ &= 1 + \left(\Delta R - \frac{d\Delta\Phi}{\sigma dQ}\right)R^{-1}. \end{aligned} \tag{74}$$

Here we noted that for the Bethe lattice $\sigma p_0 R(Q_0)=1$ and $d\Phi/dQ=\sigma R$. There are now three scenarios, depending on whether the ratio r is (a) less than, (b) equal to, or (c) greater than unity. In case (a) the discontinuity in the EOS preempts the divergence of the susceptibility and the transition is a conventional first order transition, except for a fractional power law in the EOS for p above threshold. Case (b) (consistent with the expansion up to order $1/\sigma^3$) indicates that the coincidence of the singularities in the EOS and the susceptibility is robust and survives for large but finite spatial dimension.

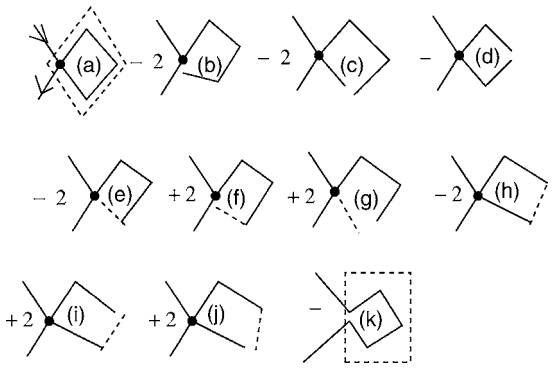

FIG. 16. Diagrams for square SQ1 of 15 on either H or B lattice. Diagram (k) occurs on the Bethe lattice but must be subtracted off because its counterpart on the hypercubic lattice has a different topology.

B. Diagrams for the susceptibility

Now we consider the effect of inserting squares or hexagons into the Bethe lattice diagrams for the susceptibility.

For squares we write

$$\Delta r_{\rm sq} = (\sigma-1)^2\frac{p^4}{2}\Delta R/R_{k-2}, \tag{75}$$

where the square insertions are discussed below. Similarly, for hexagons we write

$$\Delta r_{\rm hex} = 2p^6\sigma^3\Delta R/R_{k-2}, \tag{76}$$

where the hexagon insertions are also discussed below.

C. Percolation

As an example we first carry out the calculation for the two-point susceptibility of percolation and we confine our attention to the disordered phase, i.e., $P_\infty=0$. (The calculation for the ordered phase is quite similar.) First, consider the squares. The sum of the contributions from diagrams (a) through (j) of Fig. 16 vanishes. For diagram (k) there are $N_{\rm sq}=(\sigma-1)^2/2$ ways to attach the pseudosquare (which can be traversed in two senses). So the dashed box of diagram (k) carries the factor

$$\Delta r^{\rm SQ1} = -p^4\sigma^{-2}[1-(2/\sigma)]. \tag{77}$$

The contribution from Fig. 17 is $\Delta r^{\rm SQ2}=-(\sigma-1)^3/\sigma^5$ and that from Fig. 18 is $\Delta r^{\rm SQ3}=-(1/2)(\sigma-1)^3/\sigma^5$. So the total contribution from squares is

$$\Delta r_{\rm sq} = -(5/2)\sigma^{-2} + (13/2)\sigma^{-3}. \tag{78}$$

The contribution from hexagons is

$$\Delta r_{\rm hex} = -14\sigma^{-3}. \tag{79}$$

When these contributions are summed, one finds that the threshold for the divergence of the susceptibility agrees to order $1/\sigma^3$ with that in Eq. (16) found from the EOS and with the previous work of Gaunt and Ruskin [29]. Of course, this was hardly surprising, but the present calculation illustrates the more complicated calculation needed for k-core percolation.

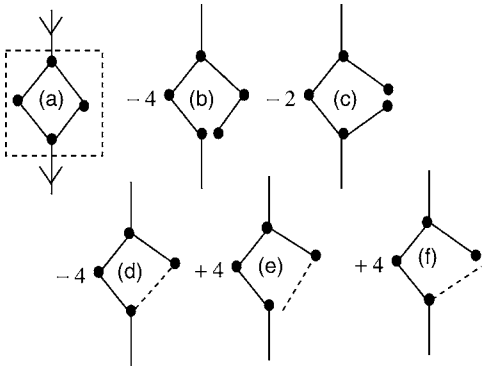

FIG. 17. Diagrams for square SQ2 of 15 on either H or B lattice.

D. k-core percolation, squares

We now consider the contributions to the susceptibility from insertions of squares as in Fig. 16. We calculate the factor ΔR associated with the dashed box. In the results given below we include the prefactors (e.g., ±2 or ±1) written in Fig. 16. We find

$$\Delta R(a) = \frac{x(\sigma-2)}{2\sigma}\{R_{k-4}^{\sigma-3}[(P^{\sigma-1})^2 + 2R(P^{\sigma-1})^2 + 3R^2P^{\sigma-1} + R^3] + R_{k-3}^{\sigma-3}[2P^{\sigma-1}(1-P^{\sigma-1}-R) + 4RP^{\sigma-1}(1-P^{\sigma-1} - R)] + R_{k-2}^{\sigma-3}[(1-P^{\sigma-1}-R)^2(1+2R) + 3R^2(1-P^{\sigma-1}-R)]\}, \quad (80)$$

where $x=(\sigma-1)^2p^4$ and we used $N_{\rm sq}=(\sigma-1)^2/2$. Also, the factor $(\sigma-2)/\sigma$ takes account of the fact that the line leaving the square has only $\sigma-2$ choices because it has to avoid the square. This factor appears for the other diagrams, except that for (b) and (f) the counting is less obvious and is discussed in Appendix A. We have

$$\Delta R(b) = -x\frac{(\sigma-2)}{\sigma}\{R_{k-2}^{\sigma-2}[1-P^{\sigma-1}(1+R+R^2) - R^3P] + R_{k-3}^{\sigma-2}[P^{\sigma-1}(1+R+R^2) + R^3P]\}, \quad (81)$$

$$\Delta R(c) = -x\frac{(\sigma-2)}{\sigma}\{R_{k-2}^{\sigma-3}(1-P)[1-P^{\sigma-1}(1+R) - R^2P] + R_{k-3}^{\sigma-3}P[1-P^{\sigma-1}(1+R) - R^2P] + R_{k-3}^{\sigma-3}(1-P) \times[P^{\sigma-1}(1+R) + R^2P] + R_{k-4}^{\sigma-3}P[P^{\sigma-1}(1+R) + R^2P]\}, \quad (82)$$

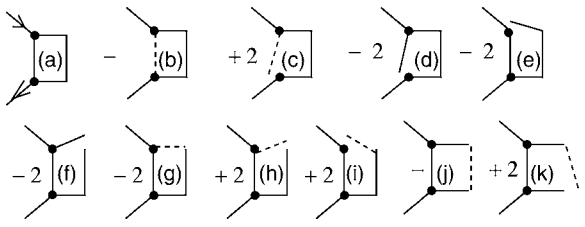

FIG. 18. Diagrams for square SQ3 of 15 on either H or B lattice.

$$\Delta R(d) = -x\frac{(\sigma-2)}{2\sigma}[R_{k-2}^{\sigma-3}(1-P^{\sigma-1}-RP)^2 + 2R_{k-3}^{\sigma-3}(1-P^{\sigma-1} - RP)(P^{\sigma-1}+RP) + R_{k-4}^{\sigma-3}(P^{\sigma-1}+RP)^2], \quad (83)$$

$$\Delta R(e) = -x\frac{(\sigma-2)}{\sigma}\{R_{k-2}^{\sigma-3}[1-P^{\sigma-1}(1+R+R^2)] + R_{k-3}^{\sigma-3}P^{\sigma-1}(1+R+R^2)\}, \quad (84)$$

$$\Delta R(f) = x\frac{(\sigma-2)}{\sigma}\{R_{k-2}^{\sigma-2}[1-P^{\sigma-1}(1+R+R^2)] + R_{k-3}^{\sigma-2}P^{\sigma-1}(1+R+R^2)\}, \quad (85)$$

$$\Delta R(g) = x\frac{(\sigma-2)}{\sigma}\{R_{k-2}^{\sigma-3}[1-P^{\sigma-1}(1+R) - R^2P] + R_{k-3}^{\sigma-3}[P^{\sigma-1}(1+R) + R^2P]\}, \quad (86)$$

$$\Delta R(h) = -x\frac{(\sigma-2)}{\sigma}[R_{k-4}^{\sigma-3}(P^{\sigma-1})^2(1+R) + R_{k-3}^{\sigma-3}(1 - P^{\sigma-1})P^{\sigma-1}(1+R) + R_{k-3}^{\sigma-3}P^{\sigma-1}(1-P^{\sigma-1}-RP^{\sigma-1}) + R_{k-2}^{\sigma-3}(1-P^{\sigma-1})(1-P^{\sigma-1}-RP^{\sigma-1})], \quad (87)$$

$$\Delta R(i) = x\frac{(\sigma-2)}{\sigma}[R_{k-4}^{\sigma-3}P^{\sigma-1}(P^{\sigma-1}+RP) + R_{k-3}^{\sigma-3}(1-P^{\sigma-1}) \times(P^{\sigma-1}+RP) + R_{k-3}^{\sigma-3}P^{\sigma-1}(1-P^{\sigma-1}-RP) + R_{k-2}^{\sigma-3}(1 - P^{\sigma-1})(1-P^{\sigma-1}-RP)], \quad (88)$$

$$\Delta R(j) = x\frac{(\sigma-2)}{\sigma}[R_{k-4}^{\sigma-3}PP^{\sigma-1}(1+R) + R_{k-3}^{\sigma-3}(1-P)P^{\sigma-1}(1 + R) + R_{k-3}^{\sigma-3}P(1-P^{\sigma-1}-RP^{\sigma-1}) + R_{k-2}^{\sigma-3}(1-P)(1 - P^{\sigma-1}-RP^{\sigma-1})]. \quad (89)$$

Also

$$\Delta R(k) = -R^5p^4(\sigma-1)^2. \quad (90)$$

So, in all from Fig. 16 we get

$$\sum_{y=a}^{k}\Delta R(y) = \frac{x(\sigma-2)}{\sigma}PR^3(R_{k-2}^{\sigma-2} - R_{k-3}^{\sigma-2}) + \frac{x(\sigma-2)R_{k-4}^{\sigma-3}}{2\sigma}(-3R^2P^2 + 3R^2P^{\sigma-1} + R^3) - xR^5 + \frac{x(\sigma-2)}{2\sigma}R_{k-3}^{\sigma-3}(6R^2P^2 - 6R^2P^{\sigma-1}) + \frac{x(\sigma-2)}{2\sigma}R_{k-2}^{\sigma-3}[3R^2(P^{\sigma-1}-P^2) - R^3]. \quad (91)$$

We next consider the contributions from the diagrams of Fig. 17. We get

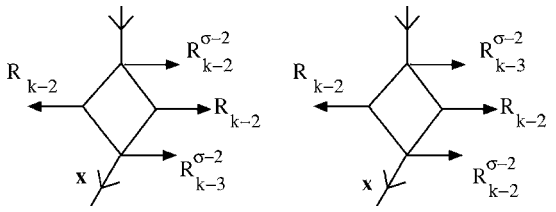

FIG. 19. Diagrams for Eq. (92). In the left-hand diagram the bottom site will be culled if the bond x is culled. In that case the entire cluster will be culled. So the stability of this cluster depends on the state of bonds below x, and therefore this diagram can be extended. In contrast, the right-hand cluster survives culling no matter what may be the state of bond x. Hence this diagram truncates and we discard it.

$$\Delta R(a) = \frac{x(\sigma-1)}{2\sigma}[2R(R_{k-2}^{\sigma-2})^2(1-P^{\sigma-1}-R) + 2RP^{\sigma-1}(R_{k-3}^{\sigma-2})^2 + R^2(R_{k-3}^{\sigma-2})^2 + R^2R_{k-2}^{\sigma-2}R_{k-3}^{\sigma-2}]. \quad (92)$$

In Fig. 19 we show the evaluation of the last term in this result. Note that for a diagram with a loop, it can matter which way the diagram is entered.

$$\Delta R(b) = -2\frac{\sigma-1}{\sigma}xR^2[R_{k-3}^{\sigma-2}(P^{\sigma-1}+RP) + R_{k-2}^{\sigma-2}(1-P^{\sigma-1} - RP)], \quad (93)$$

$$\Delta R(c) = -x\frac{(\sigma-1)}{\sigma}R[R_{k-3}^{\sigma-2}P + R_{k-2}^{\sigma-2}(1-P)]^2, \quad (94)$$

$$\Delta R(d) = -2\frac{x(\sigma-1)}{\sigma}RR_{k-2}^{\sigma-2}[R_{k-3}^{\sigma-2}P^{\sigma-1} + R_{k-2}^{\sigma-2}(1-P^{\sigma-1})], \quad (95)$$

$$\Delta R(e) = 2x\frac{\sigma-1}{\sigma}R^2[R_{k-3}^{\sigma-2}P^{\sigma-1} + R_{k-2}^{\sigma-2}(1-P^{\sigma-1})], \quad (96)$$

$$\Delta R(f) = 2\frac{x(\sigma-1)}{\sigma}RR_{k-2}^{\sigma-2}[R_{k-3}^{\sigma-2}P + R_{k-2}^{\sigma-2}(1-P)]. \quad (97)$$

So, in all we get from the diagrams of Fig. 17

$$\sum_{y=a}^{f}\Delta R(y) = -2x\frac{\sigma-1}{\sigma}(R_{k-3}^{\sigma-2}-R_{k-2}^{\sigma-2})R^3P + \frac{x(\sigma-1)R}{\sigma}(P^{\sigma-1} - P^2)(R_{k-2}^{\sigma-2}-R_{k-3}^{\sigma-2})^2 + \frac{x(\sigma-1)}{2\sigma}R^2(R_{k-3}^{\sigma-2}-R_{k-2}^{\sigma-2}) \times(R_{k-3}^{\sigma-2}+2R_{k-2}^{\sigma-2}). \quad (98)$$

For the diagrams of Fig. 18 we have

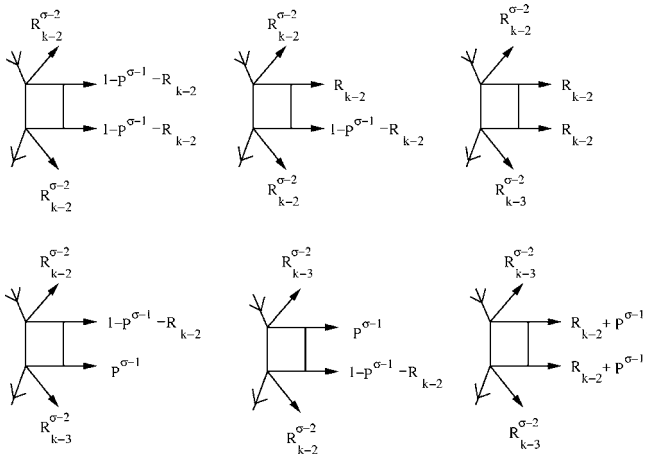

FIG. 20. Evaluation of $\Delta R(a)$ of Eq. (99).

$$\Delta R(a) = \frac{x(\sigma-1)}{\sigma}[R^2R_{k-2}^{\sigma-2}R_{k-3}^{\sigma-2} + (R_{k-3}^{\sigma-2})^2(R+P^{\sigma-1})^2 + 2R_{k-2}^{\sigma-2}R_{k-3}^{\sigma-2}P^{\sigma-1}(1-P^{\sigma-1}-R) + (R_{k-2}^{\sigma-2})^2(1-P^{\sigma-1} - R)(1-P^{\sigma-1}+R)], \quad (99)$$

as is illustrated in Fig. 20.

For the other diagrams in Fig. 18 we find

$$\Delta R(b) = -x\frac{(\sigma-1)}{\sigma}(R_{k-2}^{\sigma-2})^2R^2, \quad (100)$$

$$\Delta R(c) = +2xR^3R_{k-2}^{\sigma-2}, \quad (101)$$

$$\Delta R(d) = -2xR^3[R_{k-2}^{\sigma-2}(1-P) + R_{k-3}^{\sigma-2}P], \quad (102)$$

$$\Delta R(e) = -2xR\{R_{k-2}^{\sigma-2}[1-P^{\sigma-1}(1+R) - R^2P] + R_{k-3}^{\sigma-2}[P^{\sigma-1}(1+R) + PR^2]\}, \quad (103)$$

$$\Delta R(f) = -2x\frac{\sigma-1}{\sigma}[R_{k-2}^{\sigma-2}(1-P) + R_{k-3}^{\sigma-2}P][R_{k-2}^{\sigma-2}(1-P^{\sigma-1} - RP) + R_{k-3}^{\sigma-2}(P^{\sigma-1}+RP)], \quad (104)$$

$$\Delta R(g) = -2x\frac{(\sigma-1)}{\sigma}R_{k-2}^{\sigma-2}[R_{k-2}^{\sigma-2}(1-P^{\sigma-1}-RP^{\sigma-1}) + R_{k-3}^{\sigma-2}P^{\sigma-1}(1+R)], \quad (105)$$

$$\Delta R(h) = 2x\frac{\sigma-1}{\sigma}R_{k-2}^{\sigma-2}[R_{k-2}^{\sigma-2}(1-P^{\sigma-1}-RP) + R_{k-3}^{\sigma-2}(P^{\sigma-1} + RP)], \quad (106)$$

$$\Delta R(i) = 2xR[R_{k-2}^{\sigma-2}(1-P^{\sigma-1}-RP^{\sigma-1}) + R_{k-3}^{\sigma-2}(1+R)P^{\sigma-1}], \quad (107)$$

$$\Delta R(j) = -x\frac{(\sigma-1)}{\sigma}[R_{k-2}^{\sigma-2}(1-P^{\sigma-1}) + R_{k-3}^{\sigma-2}P^{\sigma-1}]^2, \quad (108)$$

$$\Delta R(k) = 2x\frac{\sigma-1}{\sigma}[R_{k-2}^{\sigma-2}(1-P^{\sigma-1}) + R_{k-3}^{\sigma-2}P^{\sigma-1}][R_{k-2}^{\sigma-2}(1-P) + R_{k-3}^{\sigma-2}P]. \quad (109)$$

So, in all from the diagrams of Fig. 18 we get

$$\sum_{y=a}^{k}\Delta R(y) = 4xR^3P(R_{k-2}^{\sigma-2}-R_{k-3}^{\sigma-2}) + x\frac{\sigma-1}{\sigma}\{(R_{k-2}^{\sigma-2})^2[-2R^2 + 2R(P^{\sigma-1}-P^2)] + (R_{k-3}^{\sigma-2})^2[R^2+2R(P^{\sigma-1}-P^2)] + R_{k-2}^{\sigma-2}R_{k-3}^{\sigma-2}[R^2-4R(P^{\sigma-1}-P^2)]\}. \quad (110)$$

E. *k*-core percolation, hexagons

Now consider the diagrams of Fig. 8, but for the susceptibility instead. Here and below the vertices (or vertex) which are part of the chain are indicated by filled circles. With $y=2\sigma^3p^6$ we have (with $R\equiv R_{k-2}$)

$$\Delta R(a) = y\{R_{k-4}[P^2(1+2R+3R^2+4R^3)+5R^4P+R^5] + 2R_{k-3}P[1-R^4-P(1+R+R^2+R^3)+R(1-R^3) - RP(1+R+R^2)+R^2(1-R^2)-R^2P(1+R)+R^3(1-R)-R^3P] + R[(1-P-R)^2(1+2R+3R^2+4R^3) + 5R^4(1-P-R)]\}, \quad (111)$$

$$\Delta R(b) = -2y\{R_{k-3}P(1+R+R^2+R^3+R^4+R^5)+R[1-P(1+R+R^2+R^3+R^4+R^5)]\}, \quad (112)$$

$$\Delta R(c) = -2y\{R_{k-4}P^2(1+R+R^2+R^3+R^4)+R_{k-3}P(1-P)(1+R+R^2+R^3+R^4)+R_{k-3}P[1-P(1+R+R^2+R^3+R^4)]+R(1-P)[1-P(1+R+R^2+R^3+R^4)]\}, \quad (113)$$

$$\Delta R(d) = -2y\{R_{k-4}P^2(1+R)(1+R+R^2+R^3)+R_{k-3}P(1+R)\times[1-P(1+R+R^2+R^3)]+R_{k-3}P[1-P(1+R)](1+R+R^2+R^3)+R[1-P(1+R)][1-P(1+R+R^2+R^3)]\}, \quad (114)$$

$$\Delta R(e) = -y\{R_{k-4}P^2(1+R+R^2)^2+2R_{k-3}P(1+R+R^2)[1-P(1+R+R^2)]+R[1-P(1+R+R^2)]^2\}, \quad (115)$$

$$\Delta R(f) = 2y\{R_{k-3}P(1+R+R^2+R^3+R^4)]+R[1-P(1+R+R^2+R^3+R^4)]\}, \quad (116)$$

$$\Delta R(g) = 2y\{R_{k-4}P^2(1+R+R^2+R^3)+R_{k-3}P(1-P)(1+R+R^2+R^3)+R_{k-3}P[1-P(1+R+R^2+R^3)]+R(1-P)[1-P(1+R+R^2+R^3)]\}, \quad (117)$$

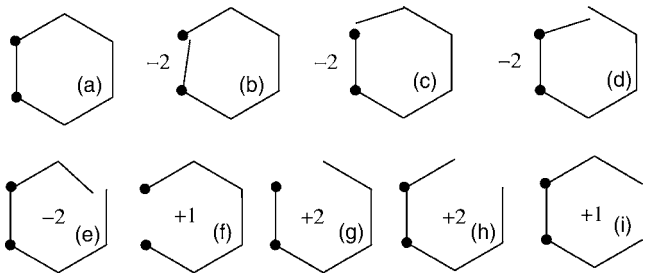

FIG. 21. Susceptibility hexagons on either *H* or *B* lattice.

$$\Delta R(h) = 2y\{R_{k-4}P^2(1+R)(1+R+R^2)+R_{k-3}P[1-P(1+R)]\times(1+R+R^2)+R_{k-3}P(1+R)[1-P(1+R+R^2)] + R[1-P(1+R)][1-P(1+R+R^2)]\}. \quad (118)$$

In addition we have the analog of diagram (k) of Fig. 16:

$$\Delta R(i) = -2yR^7. \quad (119)$$

We call the sum of these contributions $\Gamma_{H,A}$. We have

$$\Gamma_{H,A} = 2\sigma^3p^6[R_{k-4}(-5P^2R^4+5PR^4+R^5)+2R_{k-3}P(5R^4P-5R^4-R^5)-5R^5P^2+(5R^5+2R^6)P-R^6-2R^7]. \quad (120)$$

Now we consider the diagrams of Fig. 21. We have

$$\Delta R(a) = 2y\{R_{k-3}^2[P^2(1+2R+3R^2)+4PR^3+R^4] + 2R_{k-3}R[P(1-P-R)(1+2R+3R^2)]+R_{k-3}R^5 + R^2[(1-P-R)^2(1+2R+3R^2)+4(1-P-R)R^3]\}, \quad (121)$$

$$\Delta R(b) = -4yR^5[R(1-P)+R_{k-3}P], \quad (122)$$

$$\Delta R(c) = -4y\{RR_{k-3}[(1+R+R^2+R^3+R^4)P]+R^2[1-P(1+R+R^2+R^3+R^4)]\}, \quad (123)$$

$$\Delta R(d) = -4y[R(1-P)+R_{k-3}P]\{R[1-P(1+R+R^2+R^3)] + R_{k-3}P(1+R+R^2+R^3)\}, \quad (124)$$

$$\Delta R(e) = -4y\{R[1-P(1+R)]+R_{k-3}P(1+R)\}\{R[1-P(1+R+R^2)]+R_{k-3}P(1+R+R^2)\}, \quad (125)$$

$$\Delta R(f) = 2yR^6, \quad (126)$$

$$\Delta R(g) = 4y\{RR_{k-3}[(1+R+R^2+R^3)P]+R^2[1-P(1+R+R^2+R^3)]\}, \quad (127)$$

$$\Delta R(h) = 4y[R(1-P)+R_{k-3}P]\{R[1-P(1+R+R^2)] + R_{k-3}P(1+R+R^2)\}, \quad (128)$$

$$\Gamma_i = 2y\{R[1-P(1+R)]+R_{k-3}P(1+R)\}^2. \quad (129)$$

We call the sum of all these contributions $\Gamma_{H,B}$. We have

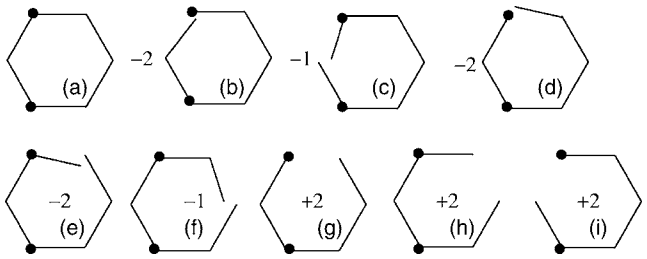

FIG. 22. Susceptibility hexagons on either H or B lattice.

$$\Gamma_{H,B} = 4\sigma^3 p^6 \{R_{k-3}^2[4R^3(P-P^2)+R^4] + R_{k-3}[8R^4(P^2-P) - 4R^5P + R^5] - 4R^5P^2 + 4R^5P + 4PR^6 - 2R^6\}. \tag{130}$$

Next we consider the diagrams of Fig. 22.

$$\Delta R(a) = 2y\{R_{k-3}^2(R^4 + 4R^3P + 2R^2P^2 + RP^2) + RR_{k-3}[2RP(1 - P - R) + 4R^2P(1-P-R) + R^4] + R^2[R(1-P-R)^2 + 2R^2(1-P-R)^2 + 4R^3(1-P-R)]\}, \tag{131}$$

$$\Delta R(b) = -4yR^4\{R[1-P(1+R)] + R_{k-3}P(1+R)\}, \tag{132}$$

$$\Delta R(c) = -2yR^3[R(1-P) + R_{k-3}P]^2, \tag{133}$$

$$\Delta R(d) = -4yR^2\{R[1-P(1+R+R^2+R^3)] + R_{k-3}P(1+R+R^2+R^3)]\}, \tag{134}$$

$$\Delta R(e) = -4yR[R(1-P) + R_{k-3}P]\{R[1-P(1+R+R^2)] + R_{k-3}P(1+R+R^2)]\}, \tag{135}$$

$$\Delta R(f) = -2yR\{R[1-P(1+R)] + R_{k-3}P(1+R)\}^2, \tag{136}$$

$$\Delta R(g) = 4yR^2\{R[1-P(1+R+R^2)] + R_{k-3}P(1+R+R^2)\}, \tag{137}$$

$$\Delta R(h) = 4yR\{R[1-P(1+R)] + R_{k-3}P(1+R)\}[R(1-P) + R_{k-3}P], \tag{138}$$

$$\Delta R(i) = 4yR^4[R(1-P) + R_{k-3}P]. \tag{139}$$

We call the sum of these contributions $\Gamma_{H,C}$. We find that $\Gamma_{H,C}=\Gamma_{H,B}$.

Next we consider the diagrams of Fig. 23.

$$\Delta R(a) = y\{R_{k-3}^2(R^4 + 4R^3P + 2R^2P^2) + RR_{k-3}[4R^2P(1-P-R) + R^4] + R^2[2(1-P-R)^2R^2 + 4(1-P-R)R^3]\}, \tag{140}$$

$$\Delta R(b) = -4yR^3\{R[1-P(1+R+R^2)] + R_{k-3}P(1+R+R^2)\}, \tag{141}$$

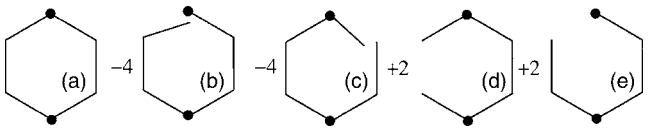

FIG. 23. Susceptibility hexagons on either H or B lattice.

$$\Delta R(c) = -4yR^2\{R[1-P(1+R)] + R_{k-3}P(1+R)\}[R(1-P) + R_{k-3}P], \tag{142}$$

$$\Delta R(d) = 2yR^2[R(1-P) + R_{k-3}P]^2, \tag{143}$$

$$\Delta R(e) = 4yR^3[R[1-P(1+R)] + R_{k-3}P(1+R)]. \tag{144}$$

We call the sum of these contributions $\Gamma_{H,D}$. We have $\Gamma_{H,D}=\Gamma_{H,B}/2$. Then the total contribution to the renormalization of R from hexagons is

$$\Delta R_{\text{hex}} = 2p^6\sigma^3\{R_{k-4}[5R^4(P-P^2)+R^5] + R_{k-3}^2[20R^3(P-P^2) + 5R^4] - 25R^5(P^2-P) + R_{k-3}[50(P^2-P)R^4 - 22PR^5 + 5R^5] + 22R^6P - 11R^6 - 2R^7\}. \tag{145}$$

VII. CONCLUSION

We now have all that we need to evaluate whether or not the perturbed ratio r, i.e., the right-hand side of Eq. (74), is unity or not to order $1/\sigma^3$. Using Eqs. (145) and (70) we see that the contributions from the hexagons do not contribute to the rhs of Eq. (74). Furthermore, using MATHEMATICA [31], we summed the contributions from the squares in Eqs. (43), (91), (98), and (110), which led to the result (at the transition in the EOS) that

$$r = 1 + (3\sigma p^4/2)R^2(R-R_{k-3})[(2-k)R + \sigma Q R_{k-3}] + O(\sigma^{-4}). \tag{146}$$

In writing this result we have assumed that the effect of $1/d$ perturbations is merely to shift the location of the pole in the susceptibility. It is not obvious that this is a correct assumption, since we do not know *a priori* that for finite d the suceptibility diverges (as it does in the other problems for which we cited the use of the $1/d$ expansion) [32]. A discussion is given in Appendix B to justify this assumption.

Since $p \sim 1/\sigma$, the term proportional to p^4 is of order σ^{-3}. Note that to leading order in $1/\sigma$ we have that

$$R_m = (\sigma Q)^m (m!)^{-1} e^{-\sigma Q}, \tag{147}$$

which implies that $(2-k)R+\sigma Q R_{k-3}=O(1/\sigma)$, so that to order $(1/\sigma)^3$, the result of Eq. (146) is that $r=1$, which means that to this order the singularity in the EOS and the divergence in the susceptibility coincide. Note that this result is not a trivial one in that it implicitly involves Eq. (147). Also, it can hardly be a coincidence that the subtleties of diagram counting lead to this result. It would not totally surprise us if this result could be obtained to all orders in $1/\sigma$ by some type of Ward identity, even in the absence of a field theoretical formulation.

The coincidence of the two singularities suggests that the unusual nature of the $k \geqslant 3$-core transition survives in large, but finite, spatial dimensions. Given the absence of numerical confirmation of such a transition in simple isotropic k-core models on square, cubic, and triangular lattices, our results motivate further numerical studies of models that are more mean-field-like in the sense that the range (number) of nearest neighbors $\sigma+1$ is larger than previous models. Of course, to compare with our results one would need to study hypercubic lattices at large d. Since "culling" leads to nonlocal truncations, it will not be easy to simulate systems at large d to check our work. However, should such a program be undertaken, one might want to have actual expressions for the shift in the critical point and the shift in the jump of the order parameter due to finite dimensionality. To get the shift in p_c, one needs to evaluate the rhs of Eq. (24), using Eqs. (43) and (70). This result will include all corrections up to and including order $1/\sigma^3$. However, it is necessary to expand the quantities such as p_0, Q_0, and R_m in powers of $1/\sigma$, as is indicated by Eqs. (17) and (29). Furthermore, to get the shift in the jump in the order parameter involves evaluating the right-hand side rhs of Eq. (26) and for this we had recourse to MATHEMATICA [31].

In order to assess the implications of our work when placed in context with known results we refer to the phase diagram in the k-d plane in Fig. 24 where we indicate existing results for k-core percolation. The two regimes which are most securely established are (a) for $k=2$ the model has [33] the same critical point as ordinary percolation and (b) for $k \geqslant d+1$ the critical concentration for percolation has been shown [20] to be $p_c=1$. The present work suggests that the hybrid transition found for $d=\infty$ persists into the regime $k \ll d < \infty$. In addition, numerical work indicates that the transition may be continuous for $k=d=3$ [15,34]. Since this is the only data point which gives a continuous transition for $k>2$, it is important to confirm this result on larger samples, although our discussion will assume the validity of this result. The $1/d$ result of the present work indicates that the hybrid transition occurs for $k \geqslant 3$ at large d, so it is clear that the continuous transition seen at $k=d=3$ must disappear as d is increased for $k=3$. The details of this boundary between hybrid and continuous transitions is unclear at present, except that it seems almost certain that $k=3$ is essentially different from $k=2$. Furthermore, at present there is no evidence of yet another phase between the hybrid phase and the $p_c=1$ phase at high d. This phase boundary might remain at $k=d+1$. Alternatively, since finite-dimensional fluctuations reduce p_c in the hybrid phase from its mean-field or Bethe lattice value, it is possible that the phase boundary between these two phase falls below the line $k=d+1$, as indicated by the question mark in Fig. 24. From the perspective of Fig. 24 it would be interesting to develop a realization of k-core percolation for noninteger k.

It is interesting to note how the $1/\sigma$ expansion for k-core percolation compares to that for other systems. For self-avoiding walks [26], the Ising model [26], spin glasses [27], and for percolation [29], the expansions for the critical value of the coupling constant involves coefficients of $1/\sigma^n$, which are rational fractions (i.e., the ratio of two finite integers). In contrast, for lattice animals one sees the appearance of the transcendental number e in the coefficients of $1/\sigma^n$ [28]. From Eq. (20) one sees a similar result for k-core percolation. It has been noted [7] that the unusual mean-field value of the correlation length exponent for k-core percolation is identical to that for lattice animals [35]. Thus, it is not surprising that these two models show similar unusual characteristics in their $1/\sigma$ expansion for the critical coupling constant.

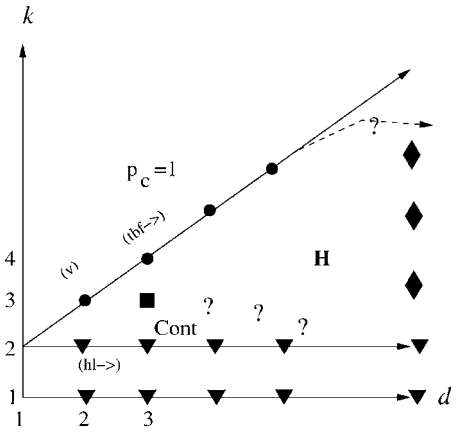

FIG. 24. Summary of known results for k-core percolation on the d-dimensional hypercubic lattice. Triangles represent ordinary percolation for $k=1$ and biconnectedness for $k=2$ (whose critical exponents are governed by the fixed point of ordinary percolation [33]). Circles represent systems for which p_c was shown to be unity for $d=2$ by van Enter [18] and by Toninelli *et al.* [20] for larger d. The filled square represents the result of Ref. [16,34] for $d=k=3$ where the transition appears to be continuous. This result therefore suggests the existence of a region labeled "Cont" of a continuous transition with a critical point probably similar to that of ordinary percolation. The filled diamonds represent the present work suggesting that the hybrid transition marked H survives for large d (but with k not comparable to d). The question marks indicate that the boundaries between the continuous transition (filled square) and the hybrid transition, as well as that between $p_c=1$ and the hybrid regime, are unclear at present.

VIII. DISCUSSION

The model of k-core percolation sets a constraint on the number of occupied neighboring bonds (or sites in the corresponding site problem). So the physics of k-core pertains to systems with nontrivial constraints such as the onset of long-range orientational order in solid ortho-para H_2 mixtures and the onset of rigidity in a mechanical system. Given the equivalence between rigidity percolation and $(g+1)$-core percolation on the Bethe lattice [12], the results here suggest that provided g is at least 2 in high dimensions, the percolation transition should be of a hybrid nature where there is a jump in the order parameter accompanied with a diverging length scale. We note that there exists a field theory [36] of rigidity percolation that exhibits a purely first-order transition, which is very different from the hybrid nature of k-core percolation. Given our results, as well as the results of SLC, it seems that this task of constructing a field theory for rigidity percolation should be revisited.

Other systems with nontrivial constraints include the dynamics of an interface separating two magnetic domains in a random field Ising model [37]. When the disorder is strong, it is likely that more than several neighbors must have flipped previously in order to propagate the interface, again, giving rise to k-core physics. However, finite-dimensional simulations of such interfaces have only uncovered ordinary percolation exponents so far [37], as opposed to some sort of hybrid transition.

While not directly related to k-core percolation, spin glasses are systems where a set of nontrivial constraints cannot all be satisfied. This property is otherwise known as frustration. Curiously enough, it turns out that the $p \geqslant 3$-spin glass model also exhibits the unusual hybrid transition in mean field with the same exponents as k-core [38]. It would also be interesting to see if a $1/d$ expansion for this system yields the same results that we find for k-core.

The physics of glass-forming liquids, the glass transition, has received a lot of intense investigation over the years yielding a wide range of approaches [39]. One approach to modeling glassy dynamics is based on kinetically constrained spin lattice models, like the Frederickson-Andersen (FA) model [40]. In this model, down spins on a lattice denote coarse-grained regions of high mobility of the liquid, while up spins denote regions of low mobility. There is a magnetic field favoring up spins creating large regions of low mobility. Therefore as the temperature of the system is lowered, more and more regions of low mobility are created eventually leading to kinetic arrest of the liquid over large time scales. An important kinetic constraint on the motion of the spins is introduced where a randomly selected spin can flip only if the number of neighboring downs spins is equal to or greater than some integer whose maximum is $\sigma+1$. This constraint models the caging effect observed in glass-forming liquids where particles become trapped by transient cages made up of their neighbors.

There is an *exact* mapping between k-core percolation and the clustering of low mobility regions in the FA model [41,42]. The mapping to k-core is not unexpected given that up and down spins can be mapped to occupied and unoccupied sites, and therefore, the kinetic constraint maps to the k-core condition. See Refs. [41,42] for details. Given this mapping, our conclusions apply to that type of lattice model, and in high d one should observe a hybrid transition at finite temperature, provided k is not comparable to d. We note that this regime may not be directly relevant for the glass transition due to the existence of finite clusters, i.e., the cube in $d=k=3$ [43]. Then the density of particles in the liquid phase is not homogeneous. However, recent experiments on metallic glasses show short-range icosahedral order even in the liquid phase so it is not clear if the density should be assumed to be homogeneous, at least over some time scale [44]. Therefore, a thorough understanding of k-core beyond mean field is of the utmost importance to understanding such transitions as the glass transition and the onset of orientational ordering in solid ortho-para H_2 mixtures, and our work seems to be the first analytic result to deal with its finite-dimensional fluctuations.

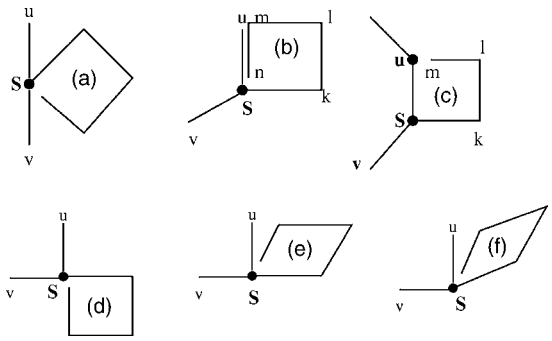

FIG. 25. Enumeration of the susceptibility diagrams for the Bethe lattice. Bonds which are parallel involve the same local displacement and sites which are close to one another coincide when the diagram is implemented on the hypercubic lattice.

ACKNOWLEDGMENTS

We thank Professor A. J. Liu for very helpful discussions. J.M.S. was supported by NSF Grant No. DMR-0087349 and Grant No. DOE-FG02-03ER46087.

APPENDIX A: COUNTING SQUARES

Here we consider in detail the counting of squares with excluded volume corrections which represent corrections of order $1/\sigma$ relative to leading corrections due to insertion of squares. More specifically, we consider the enumeration of pseudo square insertions at a single vertex, like those shown in Fig. 25. Here there are two distinct types of square insertions, all of which have to be subtracted off because their topology is different on a hypercubic lattice than on a Bethe lattice. In panel (a) the situation is simple, in that no sides of the square are equivalent to the other bonds even on a hypercubic lattice. The diagram in panel (b) has to be subtracted off, but note that because two bonds coincide on the hypercubic lattice, this diagram is in the class of diagrams of the topology of Fig. 18, which here is shown in panel (c). To avoid subtracting this diagram twice, we do not allow it in the enumeration of diagrams we wish to subtract off here. Thus we wish to enumerate pseudo squares (diagrams which would involve a square on the hypercubic lattice), but only those in which all bonds are distinct from the bonds of the chain into which the square is inserted. If the two bonds (u-S and S-v) entering the vertex are in the same direction there are of order σ^2 ways to form the square. So the number of configurations of this type is of order σ^2. We next count the number of configurations when the bond S-v is perpendicular to the incoming bond. There are then $\sigma-1$ ways to choose this bond. As shown in panels (d), (e), and (f), the square can then either (d) be in the same plane as bonds u-S and S-v (and there are two ways to do this), or (e) the square can have two bonds parallel to either bond u-S or bond S-v (there are four ways to do this) and then there are $\sigma-3$ ways to choose the other bonds of the square to be perpendicular to bonds u-S and S-v, or (f) all bonds of the square can be perpendicular to the bonds u-S and S-v (there are $(\sigma-3)(\sigma-5)$ way to do this. So in all, the number of configurations, N_s, of the square and of bond S-v is

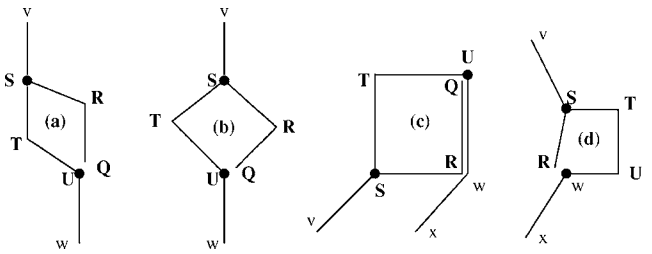

FIG. 26. Enumeration of the susceptibility diagrams for the Bethe lattice. Bonds which are parallel involve the same local displacement and sites which are close to one another coincide when the diagram is implemented on the hypercubic lattice.

$$N_s = [\sigma^2 + O(\sigma)] + (\sigma - 1)[2 + 4(\sigma - 3) + (\sigma - 3)(\sigma - 5)] = \sigma^3[1 + (4/\sigma)] + O(\sigma). \tag{A1}$$

This justifies the prefactors for diagrams (b) and (f) of Fig. 16.

The analysis for the diagrams of Fig. 17 is similar. In panels (a) and (b) of Fig. 26 we show diagrams which have a different topology on the Bethe lattice than on the hypercubic lattice and therefore which must be subtracted off. In panel (c) we show a special case when bond *Q-R* coincides with a bond (*U-w*) in the chain. As before, although we do need to subtract off this diagram, we do not include it in the present enumeration because it is of the topology of panel (d) which is included in our analysis of Fig. 18. If bond *S-T* of panel a is parallel to the incoming bond then there are $\sigma-1$ ways to complete the square and $\sigma-1$ ways to add the bond exiting the square. When bond *S-T* of panel (b) is perpendicular to the incoming bond (there are $\sigma-1$ ways to do this), there are $\sigma-2$ ways to complete the square and then $\sigma-1$ ways to add the bond exiting the square. Thus in all, N_s, the number of ways of configuring the square and the exit bond *U-w* is

$$N_s = (\sigma - 1)^2 + (\sigma - 1)(\sigma - 2)(\sigma - 1) = \sigma^3[1 - (3/\sigma)] + O(\sigma). \tag{A2}$$

This calculation justifies the prefactors for diagrams (b) and (e) of Fig. 17.

The diagrams of Fig. 18 are more straightforward because for them one does not have to consider the possibility of double counting the subtractions.

APPENDIX B: SHIFT OF SINGULARITY IN THE SUSCEPTIBILITY

In Sec. VI we evaluated the ratio r in the series for the susceptibility and interpreted the result as giving a shift in the singularity. Here we justify this interpretation. Note that the vertex renormalization (in which the unperturbed ratio r_0 is replaced by $r_0+r_0\Delta$) gives the susceptibility as

$$\chi = \sum_n r_0^n[1 + n\Delta]. \tag{B1}$$

In writing this result we noted that for a chain of n bonds the vertex renormalization could be placed at any one of order n vertices. Of course, there are end effects, so that really, if we include end effects, we would write

$$\chi = \sum_n r_0^n[1 + n\Delta + \epsilon], \tag{B2}$$

where both Δ and ϵ include all contributions of order σ^{-2} and σ^{-3}. Now we consider the contributions of *two* vertex renormalizations. If the two vertices do not interfere with one another then their contribution is $r_0\Delta^2$. For a chain of n bonds, there are of order $n^2/2$ such configurations. So in analogy with Eq. (B2), these contributions are of the form

$$\delta\chi = \sum_n r_0^n[n^2\Delta^2/2 + n\epsilon + \eta], \tag{B3}$$

where ϵ comes from configurations involving two squares or higher order configurations, none of which were counted up to order σ^{-3} in Eq. (B2). These contributions involve either one square (or hexagon) near an end point and the other in the interior of the chain, or two interfering structures in the interior of the chain. Also η comes from configurations in which all insertions are near an end of the chain.

It seems reasonable to assume that the dominant contribution to χ can therefore be written as

$$\chi = \sum_n r_0^n(1 + n\Delta + n^2\Delta^2/2 + \cdots) \to \sum r^n, \tag{B4}$$

where $r=r_0[1+\Delta]$, as we found in Sec. VI. The analysis of this appendix indicates that is appropriate to identify r as the renormalized ratio of a geometric series.

One might ask whether this identification is unique. Could the result of Eq. (B4) arise from a rounded transition for which

$$\chi = \frac{1}{2}\sum_n r_0^n[(1 + \alpha)^n + (1 + \alpha^*)^n] \tag{B5}$$

for a suitably chosen value of the complex-valued parameter α? This form of χ yields (keeping only relevant terms)

$$\chi = \sum_n r_0^n\left(1 + n(\alpha + \alpha^*)/2 + \frac{1}{4}n^2(\alpha^2 + \alpha^{*2})\right). \tag{B6}$$

For this to be of the form of Eq. (B4) we find that α must satisfy

$$\frac{1}{4}(\alpha^2 + \alpha^{*2}) = \frac{1}{8}(\alpha + \alpha^*)^2, \tag{B7}$$

which implies that $\alpha^*=\alpha$. Therefore, we cannot have a rounded transition by having the real-valued critical point for the Bethe lattice split into a complex conjugate pair of critical points (which would give a Lorentzian susceptibility with a width of order σ^{-2}). So the form of Eq. (B4) is only consistent with a shifted pole in the susceptibility, as we implicitly assumed in Sec. VI.

[1] J. Adler, R. G. Palmer, and H. Meyer, Phys. Rev. Lett. **58**, 882 (1987).
[2] S. Feng and P. N. Sen, Phys. Rev. Lett. **52**, 216 (1984).
[3] Y. Kantor and I. Webman, Phys. Rev. Lett. **52**, 1891 (1984).
[4] S. Feng, M. F. Thorpe, and E. Garboczi, Phys. Rev. B **31**, 276 (1985).
[5] A. R. Day, R. R. Tremblay, and A. M. S. Tremblay, Phys. Rev. Lett. **56**, 2501 (1986).
[6] *Rigidity Theory and Applications*, edited by M. Thorpe and P. M. Duxbury Fundamental Materials Research (Kluwer Academic/Plenum Press, New York, 1999).
[7] J. M. Schwarz, A. J. Liu, and L. Q. Chayes, e-print cond-mat/0410595.
[8] A. J. Liu and S. R. Nagel, Nature (London) **396**, 21 (1998).
[9] C. S. O'Hern, L. E. Silbert, A. J. Liu, and S. R. Nagel, Phys. Rev. E **68**, 011306 (2003).
[10] J. Chalupa, P. L. Leath, and G. R. Reich, J. Phys. C **12**, L31 (1979).
[11] B. Pittel, J. Spencer, and N. Wormald, J. Comb. Theory, Ser. B **67**, 111 (1996).
[12] C. Moukarzel, P. M. Duxbury, and P. L. Leath, Phys. Rev. E **55**, 5800 (1997).
[13] D. Stauffer and A. Aharony, *Introduction to Percolation Theory* (Taylor and Francis, London, 1992).
[14] S. Henkes and B. Chakraborty, e-print cond-mat/0504371.
[15] P. M. Kogut and P. L. Leath, J. Phys. C **14**, 3187 (1981).
[16] J. Adler and U. Lev, Braz. J. Phys. **33**, 641 (2003), and references therein.
[17] M. C. Medeiros and C. M. Chaves, Physica A **234**, 604 (1997).
[18] A. C. D. van Enter, J. Stat. Phys. **48**, 943 (1987).
[19] Even though $p_c=1$, recent results for a modified $k=3$ model on the square lattice demonstrate two new near-jammed crossover regimes as a function of occupation probability. See P. De Gregorio, A. Lawlor, P. Bradley, and K. A. Dawson, Proc. Natl. Acad. Sci. U.S.A. **102**, 5669 (2005).
[20] C. Toninelli, G. Biroli, and D. S. Fisher, Phys. Rev. Lett. **92**, 185504 (2004).
[21] G. Biroli has informed one of us (J.M.S.) about numerical results of another two-dimensional model yielding a discontinuous transition.
[22] K. G. Wilson, Phys. Rev. B **4**, 3174 (1971).
[23] K. G. Wilson and M. E. Fisher, Phys. Rev. Lett. **28**, 240 (1972).
[24] G. Toulouse, Nuovo Cimento Soc. Ital. Fis., B **23**, 234 (1974).
[25] A. B. Harris and T. C. Lubensky, Phys. Rev. Lett. **35**, 327 (1975); **35**, 1397 (1975).
[26] M. E. Fisher and D. S. Gaunt, Phys. Rev. **133**, A224 (1964).
[27] R. R. P. Singh and M. E. Fisher, J. Appl. Phys. **63**, 3994 (1988).
[28] A. B. Harris, Phys. Rev. B **26**, 337 (1982).
[29] D. S. Gaunt and H. Ruskin, J. Phys. A **11**, 1369 (1978).
[30] G. A. Baker, Jr. and L. P. Benofy, J. Stat. Phys. **29**, 699 (1982).
[31] S. Wolfram, *The Mathematica Book*, Version 4, 4th ed. (Cambridge University Press, New York, 1999).
[32] We thank Professor M. E. Fisher for pointing this out to us.
[33] A. B. Harris and T. C. Lubensky, J. Phys. A **16**, L365 (1983); A. B. Harris, Phys. Rev. B **28**, 2614 (1983).
[34] N. S. Branco and C. J. Silva, Int. J. Mod. Phys. C **10**, 921 (1999).
[35] T. C. Lubensky and J. Isaacson, Phys. Rev. A **20**, 2130 (1979).
[36] S. P. Obukhov, Phys. Rev. Lett. **74**, 4472 (1995).
[37] H. Ji and M. O. Robbins, Phys. Rev. B **46**, 14519 (1992).
[38] T. R. Kirkpatrick and P. G. Wolynes, Phys. Rev. B **36**, 8552 (1986).
[39] E. Donth, *The Glass Transition: Relaxation Dynamics in Liquids and Disordered Materials* (Springer, New York, 2001).
[40] G. H. Fredrickson and H. C. Andersen, Phys. Rev. Lett. **53**, 1244 (1984).
[41] F. Ritort and P. Sollich, Adv. Phys. **52**, 219 (2003).
[42] M. Sellitto, G. Biroli, and C. Toninelli, Europhys. Lett. **69**, 496 (2005).
[43] We thank G. Biroli for reiterating this point regarding the glass transition. In the jamming description, finite clusters in finite dimensions violate force balance.
[44] K. F. Kelton *et al.*, Phys. Rev. Lett. **90**, 195504 (2003).